MEASUREMENT ACCURACY IN CONE BEAM COMPUTED TOMOGRAPHY IN THE PRESENCE OF METAL ARTIFACT

by

Ahmed Ismail

B.Sc., Dalhousie University, 2008
D.D.S., Dalhousie University, 2012

A THESIS SUBMITTED IN PARTIAL FULFILLMENT OF

THE REQUIREMENTS FOR THE DEGREE OF

MASTER OF SCIENCE

in

THE FACULTY OF GRADUATE AND POSTDOCTORAL STUDIES

(Craniofacial Science)

THE UNIVERSITY OF BRITISH COLUMBIA

(Vancouver)

July 2020

The following individuals certify that they have read, and recommend to the Faculty of Graduate and Postdoctoral Studies for acceptance, the thesis entitled:

MEASUREMENT ACCURACY IN CONE BEAM COMPUTED TOMOGRAPHY IN THE PRESENCE OF METAL ARTIFACT

submitted by Ahmed Ismail in partial fulfillment of the requirements for

the degree of Master of Science

in Craniofacial Science

Examining Committee:

Dr. Nancy L. Ford – Faculty of Dentistry
Supervisor

Dr. Flavia Lakschevitz – Faculty of Dentistry
Supervisory Committee Member

Dr. David MacDonald – Faculty of Dentistry
Supervisory Committee Member

Dr. Vincent Lee – Faculty of Dentistry
Additional Examiner

Abstract

Purpose: Cone beam computed tomography (CBCT) image quality is known to be affected by artifacts produced by metal restorations, causing image deterioration via bright streaks and loss of gray values in the vicinity of the metallic structure. The aim of the study is to determine the impact of progressively increasing metal artifacts on the measurement accuracy of commonly evaluated points in implant treatment planning.

Methods: Holes were drilled into porcine mandibles at known distances from the alveolar crest on the buccal and lingual surfaces and filled with gutta percha. Repeated CBCT images were taken, with progressively increasing amalgam restorations and stainless-steel crowns (up to a total of 8 restorations per jaw). The imaging field of view (FOV) was of a single site (5x5cm) in 2 different locations in the mandible, as well as a full arch FOV (10x5cm). Measurement between the buccal and lingual gutta percha points on the mandible was performed using a digital caliper to establish the difference between caliper measurements compared to the same measurements taken digitally on the CBCT images. Measurements were compared under conditions with no restorations and with increasing numbers of restorations.

Results: Comparison between caliper measurements and baseline CBCT with no metal artifact demonstrated differences ranging from 0-1.7 mm. This range of variation appears to be consistent even with increasing metal artifact, with no clear detectable pattern of change. When compared to baseline measurements, scans with amalgam and stainless-steel restorations showed a maximum difference of 0.54 ± 0.64 mm and 0.62 ± 0.64 mm respectively. The change in measurements was not found to be significantly different with increasing metal restorations.

Conclusions: There may be a variation of up to 1.7 mm between measured anatomical points and CBCT imaging under commonly used settings. While this result may be clinically

important, it does not appear to be affected by increasing metal artifact due to amalgam restorations or stainless-steel crowns. The findings of this study support current clinical practices accounting for a safety margin of up to 2 mm with any CBCT image, and not limiting CBCT scans for patients with multiple metal restorations.

Lay Summary

Cone beam computed tomography (CBCT) imaging is commonly used for treatment planning dental implant cases; however, many patients have multiple metal fillings and crowns from previous dental work which are known to cause bright streaks and dark areas on the images. This study was done to determine if the accuracy of measurements changes as the number of teeth with metal increased. Repeated CBCT images were taken of pig mandibles, with gradually increasing amalgam fillings and stainless-steel crowns (up to a total of 8 metal fillings or crowns per jaw) using 2 different fields of view. Measurement between known points was performed on the mandibles using a digital caliper to establish "truth" and compared to the same measurements taken digitally on the CBCT images. While there was some difference between "truth" and CBCT images in general, this did not appear to increase with metal restorations.

Preface

This research was done and written by the author, under the supervision of Dr. Nancy L. Ford. Sourcing of the porcine mandibles was provided by Winsor Meats in Vancouver, BC. Clinical aspects of the study were done by the author, and evaluation of the images was done by the author and Dr. Ford. Part of this dissertation is planned for publication, however, at the time of writing the details of this process have not been determined yet. The abstract was submitted at conferences for the American Association of Physicists in Medicine, and the Faculty of Dentistry Research Day at the University of British Columbia.

Table of Contents

List of Tables

List of Figures

List of Abbreviations

2D	Two Dimensions
3D	Three Dimensions
AAOMR	The American Academy of Oral and Maxillofacial Radiology
ALARA	As Low As Reasonably Achievable
CBCT	Cone Beam Computed Tomography
CNR	Contrast-to-Noise Ratio
EAO	The European Association for Osseointegration
FOV	Field Of View
GV	Gray Value
ICRP	International Commission on Radiological Protection
kVp	Peak Kilovoltage
mA	MilliAmpere
MAR	Metal Artifact Reduction
μm	Micromillimeter
mm	Millimeter
PMMA	Poly Methyl Methacrylate
SRG	Seeded Region Growing
SSC	Stainless Steel Crown

Acknowledgements

First of all, I would like to offer my sincere gratitude to Dr. Nancy L. Ford, who has taught me so much about the research process from beginning to end. Your passion for teaching and empowering students shines through loud and clear. We dealt with all of the usual challenges in our three years working together, in addition to some new ones with COVID-19 and family emergencies; you have guided me through this process with compassion, grace, and enthusiasm. For that, I am forever grateful. Overall, this program has been a great experience for me to grow as a person, clinician, and researcher, and you are a very important part of that. Thank you.

I would like to thank my committee members, Dr. Flavia Lakschevitz, who was also my program director for one year and brought a fresh perspective on my education and allowed me to grow as a clinician, and Dr. David MacDonald. Your insightful comments and eagerness to be involved in my project during the committee meetings and at all times is very much appreciated. I sincerely thank you for all that you have done, it has been a pleasure to be involved with both of you for three years.

I would also like to thank some of my clinical instructors who were especially helpful during the brainstorming phase of my research journey. Dr. Mandana Nematollahi, I remember those conversations we had in first year, talking through many ideas until we had a few that came together. In addition to all your help during surgery, I especially appreciate the countless hours of your own personal time you would spend to provide feedback and advice on case planning, execution, and pushing me to get through the difficult times. A special thank you to my cousin, Ziad Saada, for your invaluable advice and assistance in using Microsoft Excel to compile, organize, and present my seemingly never-ending mountain of data.

Thank you to the UBC Faculty of Dentistry Graduate Student Research funding, and Dr. Andrea Esteves for making the Oral Health Care clinic available for our use.

Last, but not least, thank you to the graduate periodontics faculty, staff, and of course my fellow residents whom I consider a second family. These were times I will not forget, we created lifetime bonds and friendships, and you have inspired and supported me to achieve my dreams. It has been a pleasure working beside you every day in clinic and the grad lounge.

Dedication

To my mother and father, there are no words that could describe the love and pure gratitude I have for the sacrifices you have made for me…. I am forever in your debt. Both of you have always pushed me to chase my goals, no matter where they were in the world, or how much they inconvenienced you personally. These are months, years, and decades we will never get back, but through it all, I hope that I have made you proud. Ashton, thank you for being by my side, providing moral support when I needed it most, and creating a home environment for me far from home; I am excited to take these next steps in our journey together.

This is dedicated to every young teenager that ever sat in their bedroom and dreamt of a prosperous adventure and life beyond what they could imagine in a land far, far away… this is to them, the dreamers.

Chapter 1: Introduction

1.1 The current state of implant dentistry

Implant therapy for replacement of missing teeth has been researched for approximately 50 years. With the development of new rough surface implants in the late 1980s, implant survival has steadily increased and is currently estimated to be above 98% (1). However, implant survival does not necessarily imply treatment success. Even though these rough surface implants osseointegrate and provide high stability (and thus survival), they harbor greater numbers and diversity of micro-organisms than their smooth surface counterparts (2). They are also much harder to clean due to the increased porosity of their surfaces and micro-thread design (3). As a parallel to microbial insult being the trigger for periodontal disease, it is thought that microbial insult is also the trigger for peri-implantitis (4). Common signs and symptoms in an ailing implant diagnosed with peri-implantitis are inflamed gingiva, bleeding, purulence, increasing bone loss and eventual mobility of the implant. Current ranges for peri-implantitis prevalence are 14-30%, and largely depend on parameters used to diagnose the disease (5). A recent Delphi study by the European Association of Osseointegration (EAO) brought together 138 industry experts, with 75% of them agreeing that there will be an increase in peri-implant diseases by the year 2030 (6). In addition to rough surface designs, lack of access to the prosthesis for oral hygiene is another etiological factor in this disease, often due to malpositioned implants. An optimally positioned and designed implant creates a biomechanically advantageous environment for the implant and/or prosthesis to be accessible for oral hygiene management, in addition to maximizing its functional and esthetic purpose. This has culminated in an increased focus on implant planning and accuracy, as it is now recognized that the consequences of a misplaced implant are greater than during the first few decades of implant therapy.

Concurrently, in striving to improve patient outcomes, digital dentistry has been revolutionizing many aspects of clinical practice. Foremost amongst those has been implant dentistry, which has seen a reversal of the initial mindset behind treatment planning of cases in the early decades. Current thinking refers to "prosthetically-driven" treatment planning, whereby the final tooth or crown is planned in the ideal location and the implant location and angulation follows in an aim to avoid misplaced prosthetics, as opposed to placing the implant purely based on anatomy and bone availability. A major consequence of this shift towards prosthetically-driven treatment planning is the need for greater accuracy, now more than ever before. An improvement in accuracy has largely been possible due to the development of three-dimensional (3D) computer guided technology whereby planning can be completed pre-operatively and a surgical template can be fabricated to assist the surgeon based on that planning. In fact, current guidelines mandate the use of 3D imaging. According to the American Academy of Oral and Maxillofacial Radiology's (AAOMR) position statement in 2012, "the radiographic examination of any potential implant site should include the cross-sectional imaging orthogonal to the site of interest." (7) Furthermore, they recommend that cone beam computed tomography (CBCT) should be considered the imaging modality of choice for these sites. It has become clear that using only two-dimensional (2D) imaging is insufficient when it comes to implant treatment planning. In the first decades of implant therapy, 2D radiographs would be used to estimate the length of the implant to be used and adjacent root angulations, however, there would be many unknowns. Foremost amongst them are the width of the alveolar ridge buccolingually which would have to be estimated clinically prior to surgery, and can be grossly inaccurate due to the varying width of soft tissues. There are many other site-specific unknowns as well with 2D imaging, such as the precise location and path of the mental nerve, the slope of floor of the

maxillary sinus, and the presence of intrabony vessels. These are all anatomical variations that would have to be evaluated at the time of surgery, often inadequately which may lead to complications or misplaced implants in order to avoid those areas. In overcoming many of these challenges, it is easy to see why 3D technology has become ubiquitous in implant treatment planning since its introduction.

1.2 CBCT use in implant dentistry

In implant dentistry, CBCTs are currently used to assess tissue morphology, orientation, local anatomy, and pathology in the pre-surgical assessment of implant sites, bone graft augmentation sites for future implants, and post-operative assessment for failing implants. Current use goes beyond just diagnostics and involves transfer into surgery via 3D printing or live surgical navigation using the CBCT images. In particular, this is important in areas with unfavorable anatomy such as a narrow alveolar ridge, proximity to nerves, or the maxillary sinus where involvement of some anatomical landmarks could lead to serious or even life-threatening complications. One serious example of this is perforation of the lingual cortical plate and injury to the lingual artery which can cause a life threatening airway obstruction due to hemorrhage in the floor of the mouth (8). Intra-osseous arteries present in the lateral wall of the maxillary sinus are another common pitfall during maxillary bone grafting, which can be preventable with pre-operative identification and planning (9). Iatrogenic implant-related neuropathy has been reported to be increasing in populations across the world; a recent study showed that out of 30 such injuries, 90% had been planned using only traditional 2D imaging without the use of a CBCT (10). While it is important to note that CBCT implant planning does not eliminate the

risk for these complications, there is evidence to show that it can help to significantly reduce the risk.

The benefits of minimizing complication risks through CBCT imaging, however, need to be balanced with considerations for radiation risk. The ALARA (As Low As Reasonably Achievable) principle characterizes that by limiting the field of view (FOV) to as small as possible in order to minimize radiation exposure to the patient and minimize unnecessary radiation risk. Any ionizing radiation is associated with risk, however, certain tissues are more susceptible to "deterministic effects" caused by a direct impact on cell function, or "stochastic effects" caused by a mutation leading to cancer or hereditary issues. Limiting the area of exposure in the head and neck region is particularly important due to the presence of tissues that are weighted higher according to the International Commission of Radiological Protection (ICRP) (11). Examples of tissues that are relevant in dentistry are red bone marrow, thyroid gland, skin, bone surface, and the oral mucosa. Another factor to consider is that the prescribing clinician is responsible to interpret and report on the entire volume of images ordered, including any pathologies which may or may not be in their specialized field (7).

1.3 CBCT image quality

Image quality assessment is an important tool in achieving that balance between the need for high quality images and minimizing radiation to the patient. There are two broad categories of image quality assessments: observer performance tests which are often referred to as qualitative, and physical performance tests, or quantitative evaluation (12). Observer evaluation is often conducted with dry skulls, models, or phantoms and has the advantage of reflecting clinical measurements; however, they are subject to individual variations between the observer

and test objects. Physical evaluation involves measuring spatial resolution and contrast-to-noise (CNR) ratio, which provides results on an absolute scale, but, can be difficult to apply to all lesions or structures visualized.

In order to help standardize the minimum requirements for diagnostic quality CBCT while also minimizing radiation exposure, the SEDENTEXCT project was developed in the European Union in 2012 (13). Standardized phantoms were developed by the program to aid with optimizing testing for CBCT equipment, control of patient dose, quantitative image quality assessment, and the performance of the display. With respect to image quality, there are phantoms developed specifically to measure various physical image factors.

There are typically four fundamental characteristics that are evaluated when reviewing image quality: spatial resolution, contrast, noise, and artifacts. Spatial resolution is the ability to differentiate between two closely spaced objects. It is impacted by voxel size, focal spot size, and geometry of the scanner. Voxel size is the smallest image unit; theoretically, all other factors being the same, smaller voxel size results in a higher spatial resolution. However, because a smaller voxel size captures less x-ray photons per pixel, it effectively results in more image noise (14, 15). To counteract the image noise, radiation dose may need to be increased. Radiation dose increase can take place as an increase in x-ray tube current (mA) or exposure time. Some CBCT units offer control of these scan parameters as the resolution is changed, while others automate the change as the resolution is chosen (14). Pauwels et al. also note that although CBCT is considered to have a high spatial resolution, differences from machine to machine can be significant due to the use of smaller detector elements and thus smaller voxel sizes (12).

Contrast is defined as the ability of an imaging modality to distinguish various tissues in an image based on the variation in their density (12). In CBCT imaging, gray values (GVs) are often used to describe tissue density, even though there is uncertainty over the ability of these GVs to consistently reflect the actual density values. One of the factors contributing to the inconsistency is the lack of uniformity of GVs in the axial plane, where there can be a large discrepancy in GVs produced in the center of the FOV compared to the periphery. Studies have reported an average difference in GVs between central and peripheral regions of 9.5% (16). Positioning of the object seems in the axial plane seems to have an impact on the GVs and consequently, the contrast of the images produced. Studies have also shown variation in GVs due to the amount of mass inside the FOV as well as the effect of objects outside of the FOV(17). It is estimated that the presence of objects outside the FOV can shift GVs up to 10%. These studies show the importance of consistent positioning and avoiding the presence of unnecessary objects in the FOV to obtain a consistent contrast. Contrast is further influenced by several other factors including the detectable range of exposure values of the detector itself, and the display settings on the monitor (referred to as the window/level). Window width alteration is performed to optimize contrast by showing only selected GVs from the full range of values. A window of 2000 implies that 2000 GVs will be displayed only and that all values below are displayed as black, and above are displayed as white. The window level specifies the central GV within that window width, for example a window/level of 2000/0 implies that +1000 and -1000 GVs will be displayed.

Noise is the random variability in voxel values in an image owing mainly to quantum and electronic noise (12). Quantum noise is caused by the random nature of the interactions happening during x-ray production and attenuation, while electronic noise is caused by the

conversion and transmission to the detector system. Conversion refers to the process of incoming x-ray photons being converted to an electrical signal, where there can be some variability in the speed and efficiency of that process (12). Transmission refers to the signal read-out process, where different components and technologies can also affect the electronic noise produced. Noise and spatial resolution are inversely related; improving spatial resolution through smaller voxel size, for example, will typically lead to more image noise since fewer x-rays are captured by each of the smaller voxels causing the increased noise. Contrast and noise (contrast-to-noise ratio, CNR) are often used as a metric for image performance, where a higher CNR results in greater image quality.

Noise and artifacts are discussed in detail below under factors that negatively impact CBCT imaging. Other factors that can also more generally affect image quality are exposure parameters such as the FOV, beam quality (peak kilovoltage and filtration), the amount of x-rays (anode current and exposure time), and the rotation arc.

1.4 Factors negatively impacting CBCT image quality

1.4.1 Scatter

Scatter is caused by deviation of the photons from their original path between the source and the detector due to interaction with matter (18). This deviation is a result of the Compton effect and creates increased measured signal intensities, since the scattered intensities add to the primary intensity. The Compton effect results in scattered radiation produced in all directions and recorded by the pixels; however, the actual attenuation of the object within the specific x-ray beam is not recorded by the detector. The larger the detector, the higher probability that

scattered photons will impact it. The result is a reduction of soft tissue contrast and an impact on the density values of all other tissues.

1.4.2 Beam hardening artifact

Image quality can also be impacted by artifacts, which are defined as discrepancies between the subject under investigation and the reconstructed data (18). The x-ray beam emitted from the source is polychromatic, meaning that it is composed of x-ray photons of many different energies, with the maximum being equal to the peak kilovoltage (kVp) setting selected (19). As the beam passes through the subject, lower energy photons are absorbed, and are attenuated or removed from the beam. Therefore, the beam that reaches the detector is composed of a greater percentage of higher energy photons compared to the beam originating from the source, often referred to as a "hardened" beam. The denser the subject and the higher the atomic number it is composed of, the larger proportion of attenuated x-rays. The mathematical algorithm that processes information from the detector and reconstructs the image assumes a monochromatic beam, or a beam composed of x-ray photons of a single energy. The discrepancy between the assumed and actual energy of the beam, causes the algorithm to misinterpret the amount of attenuation that occurred, and assigns that area an incorrectly low gray scale value (19). These artifacts typically present as characteristic dark areas and streaks commonly seen in radiographic images, either masking underlying structures or providing false information regarding density and morphology of the subject.

1.4.3 Extinction artifact

Extinction artifact is commonly referred to as "missing value artifact", whereby the object studied contains material with a high atomic number, causing the signal intensity recorded in the detector behind that material to be zero or close to zero (18). The main interaction is

through the photoelectric effect, and extinction happens because all the energy by the incoming photons is absorbed. This also impacts surrounding tissues which would also have missing values in the reconstruction data. Prosthetic crowns, amalgam fillings, implants, orthodontic brackets, and endodontic filling are common sources of highly absorbing material. The thicker the material, or presence of multiple objects would lead to a more severe artifact.

1.4.4 Ring artifact

Ring artifacts present as concentric rings in the image centered around the axis of rotation. They are caused by defective or uncalibrated detector elements (19). They appear as rings due to the circular trajectory of the source, and typically present in axial slices.

1.4.5 Motion artifact

Motion artifacts present as shading or streaking in the reconstructed image, commonly presenting as a double image or ghost image (18). In the craniofacial region, this often results in double outlines of corticated surfaces or the posterior border of the tongue. They can result from either movement or misalignment of the subject. It has been reported that hemodynamics resulting from the heartbeat alone can cause a slight but relevant motion of the craniofacial area, estimated to be approximately 80 μm per heartbeat (13). Kiljunen *et al*. estimate the optimum spatial resolution to be approximately 500 μm in clinical practice due to all of these factors (13).

1.5 Accuracy and reliability of dental CBCT

The need for an accurate and carefully considered implant position, in addition to intra-surgical accuracy based on the anatomic landmarks discussed, bring to light the implications of errors. These errors are most commonly in the form of measurement error during the planning process, or a production error if a surgical template (or guide) is used. Accuracy in measurement

error is the ability of that measurement made on the CBCT image to be correct anatomically on average, whereas reliability is the ability of that measurement to be reproducible when repeated (20). It can be expected that the presence of artifacts or the production of a lower quality image, would result in measurement errors and therefore have an impact on their accuracy and reliability.

Several studies have reported on the accuracy and reliability of CBCTs by scanning dry skulls to complete linear measurements. One study of 10 dry human mandibles reported these measurements to be both accurate and reliable, with a mean underestimation of 0.41 mm compared to measurement of the actual distance with a digital caliper (referred to as the gold standard) (21). Another study of 13 dry human mandibles found a mean difference of 0.4 mm when measuring the incisal edge of a tooth to the cemento-enamel junction, and a mean difference of 0.6 mm when measuring the incisal edge to the alveolar bone (22). A third study of 12 dry human mandibles assessed measurements at the alveolar crest under different voxel dimensions of 0.2, 0.3 and 0.4 mm (23). They reported high accuracy and reliability for all voxel sizes, with the least amount of intra-examiner error found for 0.2 mm voxel size as would be anticipated. The range of error when compared to physical measurement was 0.08 mm to 1.14 mm, with the highest errors reported in the anterior mandible region under 0.4 mm voxel, leading the authors to suggest a higher spatial resolution (0.2 mm voxel) to be used for that anatomical region. It is intuitive that measurement precision is related to image resolution, however the need for increased resolution must be balanced with the ALARA principle.

A common issue with many of these studies, however, is the lack of soft tissue component in their experimental model, which of course does not correlate to human anatomy with soft tissues. Studies that look at a skull only, as opposed to the realistic alternative of a

head and neck with soft tissues, are expected to show a more consistent image because only high density (bone) structures are present. There would theoretically be less attenuation (or reduction in the intensity of the x-rays due to absorption or scatter when traversing matter) of the x-ray photons due to the lack of soft tissues, resulting in less scattered radiation and ultimately a higher quality image (24) . The first study to include soft tissues in their experimental model was Ganguly *et al.*, whereby they sectioned six cadaver heads to introduce radiopaque markers before taking the CBCT and left the soft tissue intact (25). They found no significant difference between physical and CBCT measurements, reporting a mean difference of 0.3mm. Another study evaluated linear measurements in 6 cadaver heads with soft tissues intact, reporting mean differences of 0.040 ± 0.27, 0.19 ± 0.84, and 0.02 ± 0.54 mm for measurements at 3 areas on the mandibular condyle, using consistent anatomical landmarks (26).

Perhaps the most clinically relevant study evaluated 18 healthy subjects that were candidates for extraction and immediate implant placement at 39 sites (27). This allowed for pre-operative evaluation of the width of the bone that is buccal to the tooth to be extracted under CBCT imaging followed by physical measurement of that bone after extraction. They found that the CBCT measurements were underestimated in 16% and overestimated in 77% of sites. With increasing thickness of the bone, the error was found to decrease considerably (correlation coefficient of 0.597 with bone width ≤1 mm compared to 0.939 with a width >1 mm). The mean error reported overall was 0.28 ± 0.29 mm. While some of these studies report statistical significance, they all show that it is safe to assume an error of less than 1 mm from a clinical perspective. This is put into practice by many of the implant planning software programs through the installation of a 1-2 mm alarm system to notify the user when they are approaching that distance from a noted anatomical landmark.

1.6 Metal artifact reduction (MAR)

Metal objects in the form of dental restorations, crowns, orthodontic brackets, or endodontic fillings are commonly encountered in the craniofacial region. By reducing contrast, obscuring structures and impairing detection of the region of interest, metal artifacts inherently make diagnosis of anatomic structures and measurements difficult and time consuming. It can be expected that there may be an effect on the accuracy and reliability of these evaluations discussed above, in the presence of metal artifacts. Many approaches in the image acquisition to try and avoid metal artifact have been discussed in the literature (28)(29). Initially, one solution was to alter the angulation of the primary beam by tilting the gantry angle during the scan to avoid the metal object(s); however, with increased incidence of restored teeth and often times the region of interest being adjacent to those restorations, the effectiveness of that strategy proved to be limited. Another approach was to alter the scan parameters by increasing the beam energy (kVp), the number of x-rays (by increasing mA or scan time), or the scan arc. The downside of this approach, however, is that it effectively increases the radiation dose to the patient. Finally, a third broad category is post-processing techniques, which involves metal artifact reduction (MAR) after the scan is taken.

There are two main strategies for these post-processing algorithms. The iterative reconstruction method attempts to recover missing or incomplete data from the original data by using a mathematical algorithm to repeatedly fill in the data on the reconstructed image (30). Statistics of projection uncertainty are used to allow flexible modelling of the image. While effective in reducing the image artifact, they are computationally expensive to employ and thus impractical for clinically used CT scanners.

The second strategy is projection-correction, which is designed to correct portions of the data distorted by the metal artifact on the raw projection images. Missing or incorrect data are completely replaced by artificial data obtained through pattern interpolation, recognition, or prediction. The effectiveness and accuracy of this strategy depends on which corrupted portions of the image are identified and the quality of the correction. Several authors indicate that because the metal artifact is a combination of beam hardening, partial volume and extinction artifact, correctly identifying faulty projection data is difficult (30). This difficulty in identifying faulty data becomes compounded with increasing numbers of metal objects.

While many CBCT manufacturers today are providing a MAR tool in their equipment or software, the results from scientific studies are currently conflicting. Bechera *et al* tested the MAR algorithm and software provided by a CBCT manufacturer (Picasso Master 3D; Vatech, Hwaseong, Republic of Korea) by evaluating CNR under different scan conditions with and without the algorithm using phantoms (29). They found that CNR was increased, and image quality was improved when the MAR option was selected. However, they concluded that they cannot show if the MAR algorithm actually restores the content of the images, or if the software simply produces values to fill in the missing gray values. Meanwhile, de-Azevedo-Vaz et al. found no impact on the diagnosis of clinical entities with or without the MAR protocols provided with their CBCT manufacturer (Picasso Trio; Vatech, Hwaseong, Republic of Korea) (31). Similarly, Kamburoglu et al. evaluated four different protocols (without MAR, and with low, medium, and high MAR) with the ProMax 3D Max machine (Planmeca Oy, Finland) and found no impact in diagnosis. One possible explanation for the variance in results is that better image quality as measured by CNR does not necessarily translate to improved diagnostic accuracy. However, the artifacts that are produced themselves may also vary under different conditions.

Interestingly, a study that looked at metal artifact from endodontic fillings at regions of interest that were exactly the same but scanned with four different CBCT machines found that the variation of artifact expression was significantly different as evaluated by three trained and calibrated dentomaxillofacial radiologists (32). There was disagreement among the evaluators as to which CBCT machine and settings produced the highest quality image, even with MAR algorithms applied with one of the units. This demonstrates that even with quantitative improvements, there is a subjective element to image evaluation.

As a consequence of this uncertainty in objectively evaluating images with metal artifact, there are no current guidelines or modifications recommended for clinicians when treatment planning a patient with multiple metal restorations. It is common for a prosthodontist or periodontist to have many patients in their practice presenting with all or the majority of their teeth restored with full coverage restorations such as porcelain fused to metal. It is also not uncommon for those patients to lose teeth due to fracture, caries, or periodontal disease and require one or multiple implants. As many of those clinicians have encountered, attempting to evaluate a CBCT image in those circumstances can be very difficult. The motivation for this study is to objectively evaluate the impact that these metal artifacts can have on measurements used in implant treatment planning, under commonly used settings. By sequentially increasing the number of restorations while repeating the same measurements, the impact of these added restorations past a certain threshold number or type (amalgam vs full coverage crowns) may be established for clinical use.

1.7 Research objectives

The hypothesis of this study is that as the number of metal restorations increase, the accuracy of the measurements will decrease. To test this hypothesis, our study will aim to:

1) Establish the difference between caliper measurements made on porcine jaws to the same measurements made digitally on the CBCT images with no restorations, in order to estimate the accuracy of measurements on the Carestream 9300 machine under commonly used settings.
2) Determine the impact of progressively increasing metal artifacts via amalgam restorations and stainless-steel crowns on linear measurement accuracy of known anatomic landmarks. The impact of several other variables will also be evaluated:
    a. Full arch (10x5 cm^2) and single site (5x5 cm^2) FOV
    b. A single site FOV with the metal restoration(s) inside the FOV and outside of the FOV.
    c. Altered CBCT scanning protocols, targeting increased kVp and scan time to evaluate if the improved image quality impacts measurement accuracy.
    d. Manual measurements in two software packages commonly used in implant dentistry: CS9300 and DTX studio, as well as a third software commonly used in preclinical research, MicroView. MicroView also allowed comparison of semi-automated measurements to the manual measurements of MicroView, CS9300, and DTX studio, in order to estimate the accuracy of selecting the measurement points visually.

Chapter 2: Experimental Methods

2.1 Overview of research project

As described in the introduction, a common measurement made in implant treatment planning is the distance between the buccal and lingual plate. To enable consistent points of measurement from an experimental perspective, fiduciary markers composed of gutta percha were added to each surface. In order to evaluate the impact of metal artifact on the accuracy of that measurement on a CBCT image, the distance anatomically on the porcine jaw had to be measured between those markers. These measurements were then repeated on CBCT images taken of the jaws with no restorations placed. Afterwards, progressively increasing number of metal restorations were added to each jaw, up to a total of 8 restorations per jaw. This was accomplished using amalgam occlusal restorations and stainless-steel crowns (SSC), in an attempt to evaluate the impact of different restorative materials present in a clinical situation (amalgam, SSC) and the surfaces they cover (occlusal only vs full coverage crown). The measurements were made on two different software packages commonly used in clinical practice, in addition to a third that allows for semi-automated selection of points of interest, to determine if there is human error in selecting consistent points of measurement. Finally, scan parameters such as increased kVp and scan time were increased, which should improve image quality by increasing beam quality and the amount of x-rays respectively, and perhaps impact the measurements. An overview of the experimental design can be seen in Figure 1.

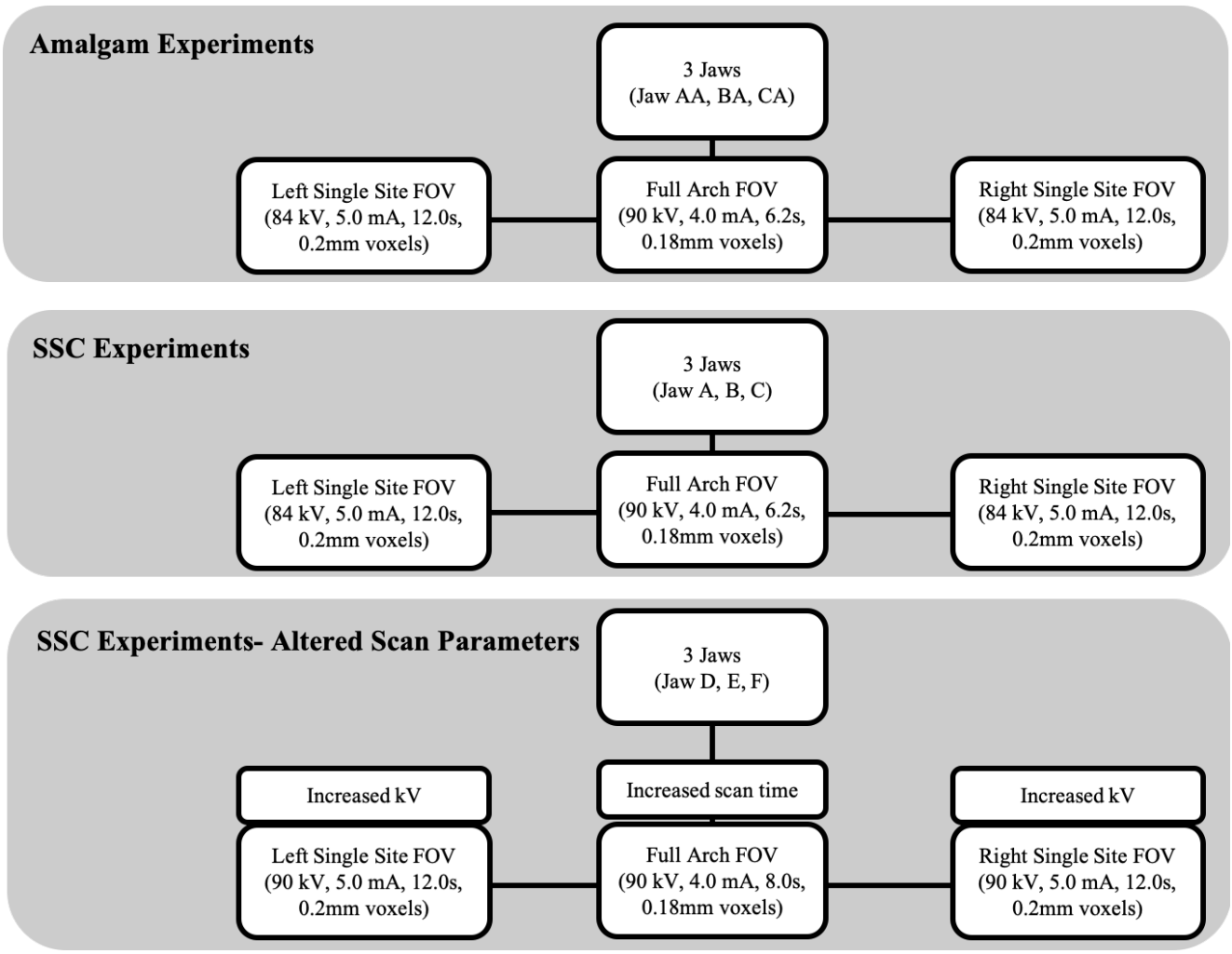

Figure 1. Flowchart illustrating an overview of the experiments.

2.2 Porcine model

Porcine mandibles were sourced from a local butcher (Windsor Meats, Vancouver, Canada), and an attempt was made to select mandibles from pigs that were of similar size, since the age and gender of the pigs could not be determined through the vendor. The maximum width that fits in the CBCT scanner without interfering with the rotation of the gantry is 17cm. A plastic container that was 16x16cm was selected to fit within that limit, and based on human head size. All mandibles were trimmed to 6 inches (152.4 mm) in length to fit within the container. The right and left side were also sectioned from each other to allow for consistent positioning and a spatial orientation more similar to the human anatomy. The average distance between the first molars on the right and left side in humans is estimated to be 44 mm (33); as such the right and left porcine jaws were positioned at 44 mm from each other. Styrofoam dividers were taped inside the container to enable consistent positioning of the mandibles, as shown in Figure 2. Large Ziplock bags were used to transfer the mandibles as well as keep the container and Styrofoam dividers clean. The mandibles were stored in a freezer at -18ºC to maintain them while not in use.

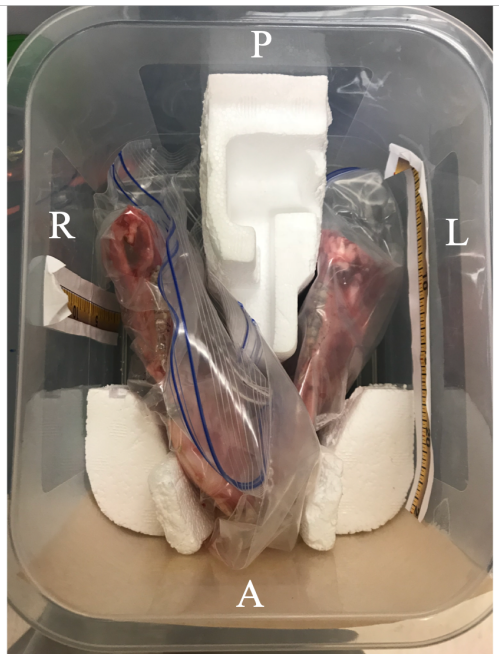

Figure 2. An occlusal view of the positioning of the right (R) and left (L) side of the porcine mandible in the plastic container using styrofoam dividers. The anterior (A) and posterior (P) aspects are also shown.

2.2.1 Adding fiducials and anatomical measurements

In order to have a consistent point of measurement both anatomically and on the CBCT images, fiduciary markers were added to each jaw. A dental material, gutta percha (Kavo Kerr, Brea, USA), was used due to its radiopaque quality enabling identification on the CBCT images, ease in modifying size and shape, and clinical relevance in that it is commonly used for endodontic restorations. To place the gutta percha points that will be measured, intrasulcular incisions were made at the first and second premolar, followed by a midcrestal incision connecting the two teeth and vertical releasing incisions for access. A full mucoperiosteal flap was raised on both the buccal and lingual aspects. A highspeed dental handpiece

(MASTERmatic LUX M25 L Highspeed, KaVo Kerr, Brea, USA) was used to drill small 1 mm holes at 3 mm, 6 mm, and 9 mm from the alveolar crest on both the buccal and lingual plates. The System B Cordless Endodontic Obturation System (Kavo Kerr, Brea, USA) was used to place and contour gutta percha points into the holes that were prepared, as shown in Figure 3. The distance between the buccal and lingual gutta percha points at 3 mm from the crest was measured ("GP-1") using a digital caliper (Tacklife, Atlanta, USA). This was repeated for the gutta percha points at 6 mm ("GP-2") and 9 mm ("GP-3") from the alveolar crest. The flaps were then reapproximated to the buccal and lingual plates, however, no sutures were used. These steps were all repeated for the opposite side of the jaw.

Figure 3. Full mucoperiosteal flap raised between the first and second premolar; placement of 3 mm gutta percha points at 3, 6, and 9 mm from the alveolar crest.

2.3 CBCT machine

The CS 9300 (Carestream Dental LLC, Atlanta, USA) at the Faculty of Dentistry, University of British Columbia was used for all scans. The right and left sides of the mandible were placed into the plastic container and secured with the styrofoam dividers. The container was then positioned on top of a mount of polymethyl methacrylate (PMMA) which was attached to a metal tripod, to be within the field of view to scan the mandibles. At baseline and after each restoration was added, three scans were taken. A 10x5 cm^2 FOV was selected since it is commonly used for full arch implant treatment planning and all cases where a digitally designed surgical guide is used. The default setting at this FOV for an adult patient was used: 90 peak kilovoltage (kVp), 4.0 milliampere (mA), 6.20 seconds and a voxel size of 0.18 mm. A single-site FOV was also selected since it is often used for evaluation of single site implant placement. Two scans were made at 5x5 cm^2 FOV, one with the left side of the jaw, followed by the right side. The default setting at this FOV for an adult patient was used: 84 kVp, 5.0 mA, 12.0 seconds, and a voxel size of 0.2 mm. Since metal objects outside of the FOV but within the path of the scan can create scatter, single site scans were also reproduced with restorations on the opposite side of the jaw, referred to as outside the FOV. Restorations were always progressively added to the left side first, up to a total of four followed by the right side for a total of eight restorations per jaw. This order of adding restorations allowed for evaluation of the right side (or outside the FOV) while the restorations were only on the left side.

2.4 Adding amalgams and CBCT scans

Once the baseline images (no restorations) were acquired, the experimental stage of adding amalgam restorations began. This involved using a highspeed dental handpiece to

prepare the first premolar on the left side of the porcine jaw with a single surface occlusal cavity preparation. The dimensions of the preparation were 3 mm in depth and followed the contour of the pits and fissures as is standard in typical single surface occlusal preparations. The restoration was then placed using fast set amalgam alloy (Dispersalloy Double Spill Fast Set, Dentsply Sirona, York, USA) which was mixed using a dental amalgamator (Silimat S5, Ivoclar Vivadent, Schaan, Liechtenstein) as per the manufacturer's instructions for 6 seconds. Excess was removed and an occlusal restoration was carved using dental hand instruments.

The left and right sides of the mandible were then placed in the individual Ziplock bags and positioned in the plastic container with the styrofoam dividers. The mount was then positioned as described above in Section 2.4.2 and a full-arch FOV image was acquired using the protocol described in Section 2.2. This was followed by two single-site FOV images, one on the left side, with the restoration inside the FOV and one on the right side with the restoration outside the FOV.

These steps were then repeated for the placement of a restoration on the left side of the jaw on the second, third, and fourth premolars with three images acquired in between each restoration placement. Once the four restorations on the left side had been scanned, the process was repeated for the right side in the same order for a total of 8 restorations per jaw and 24 images per jaw. This was repeated for 3 separate jaws, for a total of 72 images. A flowchart showing the sequence of image acquisition can be seen in Figure 4.

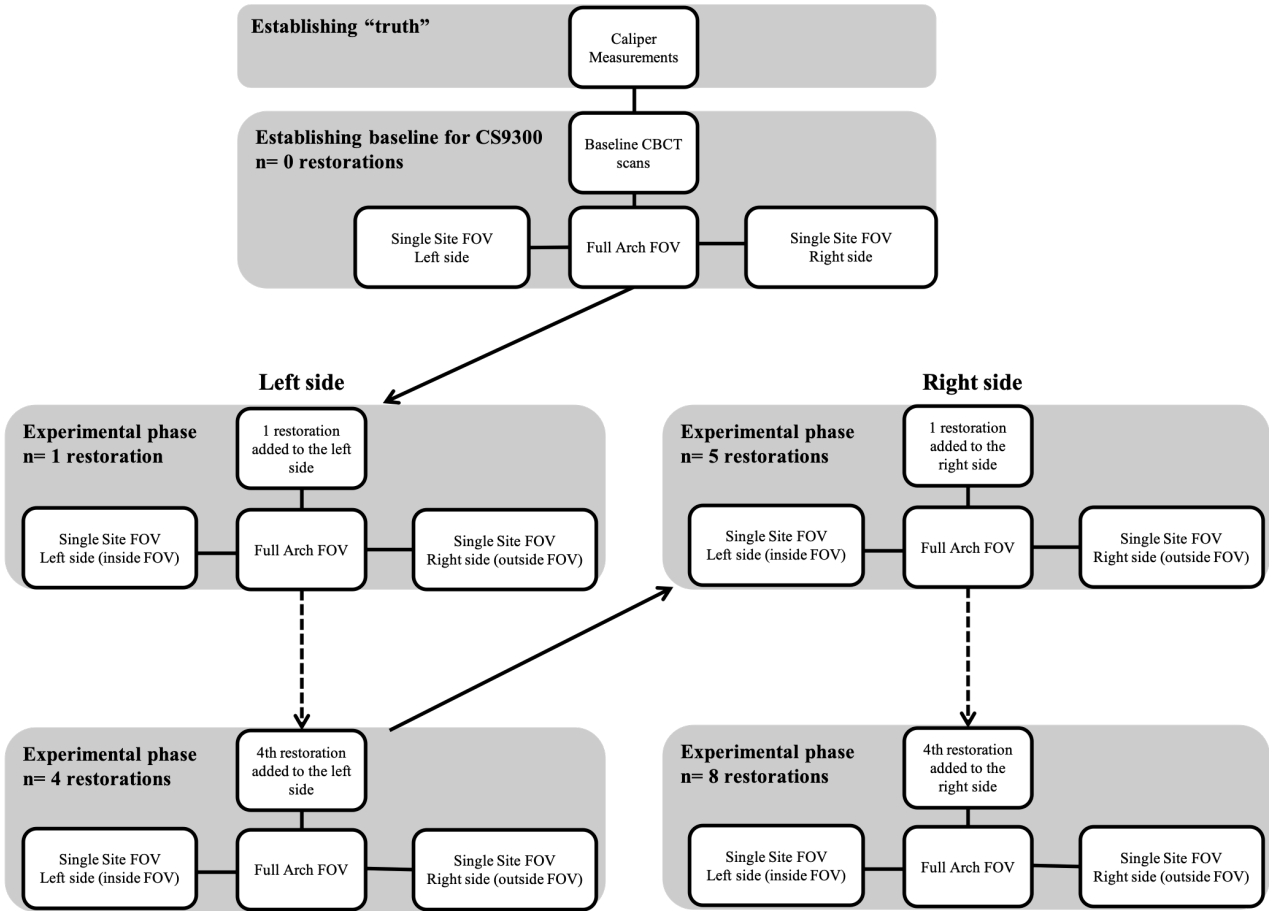

Figure 4. Flowchart illustrating the sequence of experimental data acquisition. For each jaw, caliper measurements are followed by baseline CBCT scans with no restorations in the full arch FOV and single site FOV of the right and left sides. Restorations (amalgam or SSC) are added sequentially to the left side first, followed by the same three CBCT scans after each restoration is added. Once four teeth have been restored on the left side of the jaw, the same process is repeated on the right side. A total of 8 restorations are added per jaw, with 24 CBCT images acquired in addition the three baseline images.

2.5 Adding crowns and CBCT scans

Three unique jaws were sourced, trimmed, had fiducials added, and scanned with no restorations as per section 2.3. A highspeed dental handpiece was used to perform a crown preparation with an occlusal and interproximal reduction to allow fitting of a preformed stainless-steel crown (3M Dental, St Paul, USA) on each tooth. Size of the crowns were chosen based on approximate fit to the porcine teeth. Size D2LR was used on the first premolar, D3UR for the second premolar, E2UL for the third premolar, and E5LR for the fourth premolar. Figure 5 shows one side of a jaw with all four stainless-steel crowns placed. The protocol of image acquisition described above for amalgam restorations in section 2.4 was followed for a total of 72 images.

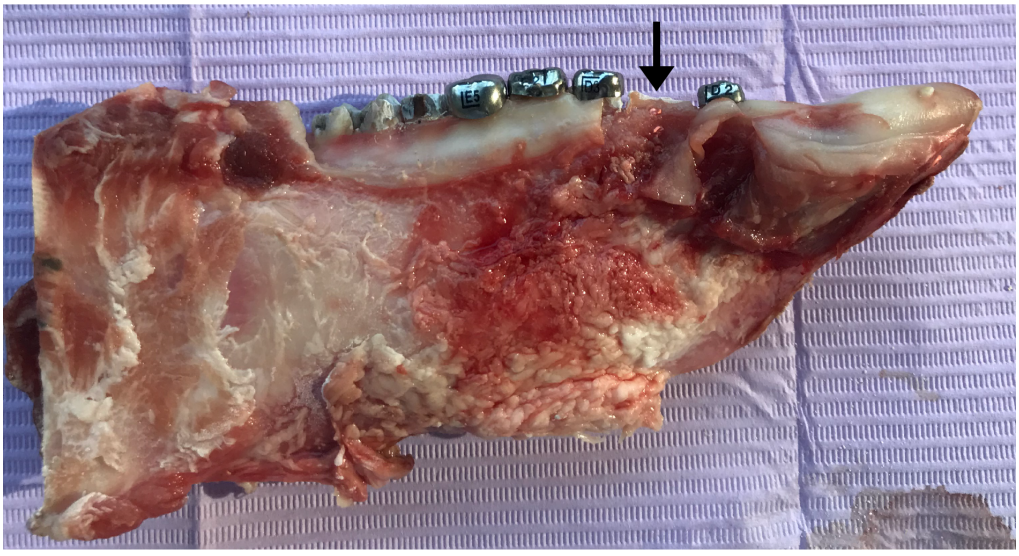

Figure 5. The left side of Jaw C with all four stainless-steel crowns placed; arrow is depicting the location of the gutta percha points.

2.6 CBCT scans with altered scan parameters

Three more unique jaws were sourced, trimmed, had fiducials added, and scanned with no restorations as per section 2.3. Crown preparations and fittings were performed as described in section 2.5, however, the scan parameters were altered in comparison with the three previous jaws. Increasing peak kilovoltage will result in higher energy and improved penetration of the x-ray beam (beam quality), and therefore improve image quality. Increasing scan time will result in an increased number of projection images, which will improve angular spacing and coverage around the metal object, and be expected to also improve image quality. The single-site kVp was increased from 84 kVp to 90 kVp while all other scan parameters were not altered. The full-arch scan time was increased from 6.2 seconds to 8.0 seconds while keeping all other scan parameters the same. A total of 72 more images were scanned.

2.7 Image analysis

Each acquired image consisted of 6 gutta percha points on the left and 6 points on the right side of the jaw. As described in Section 2.4.1, the distance between the gutta percha points at 3 mm from the alveolar crest was annotated as “GP-1”, and those at 6 mm were “GP-2”, followed by 9 mm from the crest “GP-3”. Thus, for each image there were 3 measurements per side (left and right).

2.7.1 CS 3D imaging

Data evaluation was performed using CS 3D Imaging (Carestream Dental LLC, Atlanta, USA) since it is the native program provided with the CS9300 CBCT machine (Carestream Dental LLC, Atlanta, USA) and is often used for implant treatment planning. Initially, several images were evaluated in order to choose thresholds for window and level that allows for

appropriate visualization of the anatomy and gutta percha points. Consistent window and level thresholds were selected (window 11171 and level 5367 were selected to view all images). Under the curved slicing view, the distance tool was used to manually select the buccal aspect of the buccal gutta percha point and the lingual aspect of the lingual gutta percha point. This was also repeated for all points and recorded accordingly.

2.7.2 DTX implant studio

The second software selected was DTX Implant Studio (Nobel Biocare, Switzerland) to provide relevance to implant site evaluation in clinical practice. Under the 3D planning function, the distance tool was used to manually select gutta percha points as described in Section 2.7.1. This was repeated for all points and recorded accordingly.

2.7.3 MicroView

MicroView (Parallax Innovations, Ilderton, Canada) was selected for data evaluation due to its capability in providing both manual selection points for measurement as well as semi-automated points. The software allows the user to browse through the slices of the CBCT scan and to manually identify two points to measure between. To allow for consistent visualization of the grey values, a threshold between window 11000-12000 and level 5000-6000 was set for all images. After manipulating and magnifying each image, the buccal aspect of the buccal gutta percha point and the lingual aspect of the lingual gutta percha point were selected and the distance was recorded. An example of this is shown in Figure 6.

The software also allows for semi-automated measurements. Image segmentation to identify the boundary of the gutta percha points was performed using the seeded region growing (SRG) function in MicroView. This function allows the user to select a "seed point" or pixel where the gutta percha is, and is followed by "region-growing" whereby the program identifies

pixels that are connected with gray values above the threshold that was set by the user. A threshold level of 11000, and window of 0 was set for all images. This provided a semi-automated method to identify the gutta percha points based on their grayscale values in comparison to adjacent structures. After segmenting each gutta percha point, the software provided a volume for the gutta percha and identified the center of that volume. The distance between the center of each gutta percha point was measured in a similar fashion to the manual measurements. Assuming a perfect sphere created by the gutta percha point, the radius of the sphere can be calculated using the formula for the radius as follows:

$$r = ((\frac{V}{\pi})\frac{3}{4})^{1/3}$$

where *r* represents radius and *V* represents volume. Adding the distance between the two centers of the gutta percha points to the radii of each gutta percha point should result in a semi-automated measurement comparable to that obtained using the manual measurement. The reason for this calculation is that the manual measurements are measuring the "outside" or buccal surface of one gutta percha point to the other, whereas the semi-automated measurement only provides the distance from the center of each point to the other.

2.8 Statistics

Using Prism 8 (Graphpad, La Jolla, USA), a one-way analysis of variance (ANOVA) and post-hoc Dunnett multiple comparison was performed to assess 1) the increased number of restorations compared to a control group of no restorations, 2) full arch and single site FOV, 3) single site FOV with the restoration inside and outside the FOV, and 4) measurements made in MicroView, DTX and CS9300. Statistical significance was set at $p<0.05$.

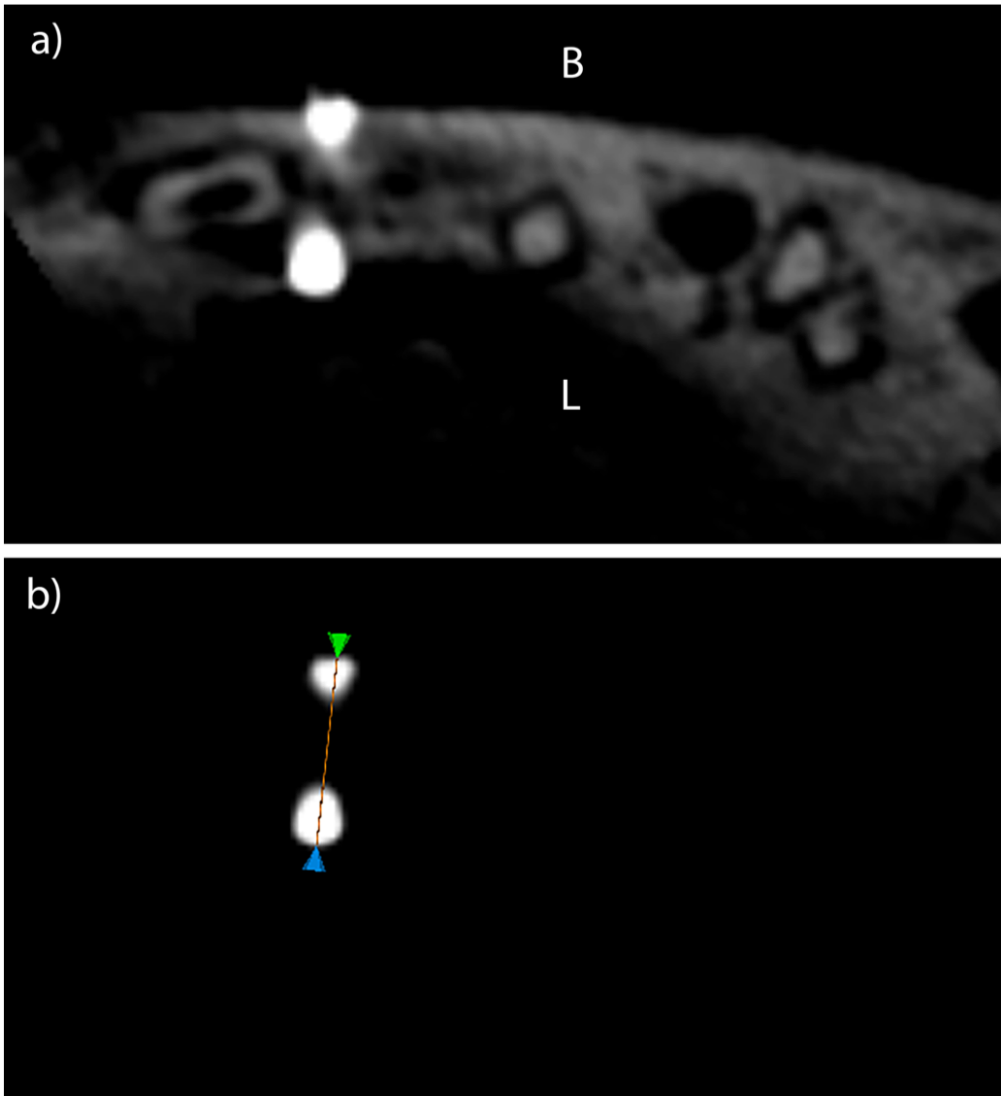

Figure 6. CBCT images from MicroView displaying gutta percha points at 3 mm from the alveolar crest at (a) commonly viewed settings; the buccal surface of the mandible is marked as, B, and the lingual surface is marked as L. The same image (b) after using the window and level function to eliminate gray values below a threshold in order to display the gutta percha points only and using the measurement tool to measure the distance.

Chapter 3: Results

3.1 Data evaluation

All images were evaluated and distances measured in the three software packages. Figure 7 shows an example of images from MicroView of the full arch FOV with (a) no metal artifact in the form of restorations present, and (b) maximum amount of metal artifact present with a total of 8 restorations.

Evaluating the measurements as raw distances measured in millimeters allows for comparison between that same measurement repeatedly as the restorations increase. However, it does not allow for comparison of that distance to others made in the same jaw at another location, for example more apical or in the opposite side of the jaw. In order to account for anatomical variability in the distance between the buccal and lingual alveolar plates within a jaw and amongst other jaws, the raw distances were subtracted from the measurements made on the baseline CBCT. A difference of zero would mean that the caliper measurement and measurement on the CBCT image are identical. A positive value indicates that the distance is overestimated on the CBCT image, while a negative value indicates that the distance is underestimated on the CBCT image.

It is important to note that absolute values were used to calculate averages of the differences. This was done since this study seeks to answer the question of whether there is a difference between having metal restorations and not having them in the CBCT image, rather than the directionality of positive or negative difference.

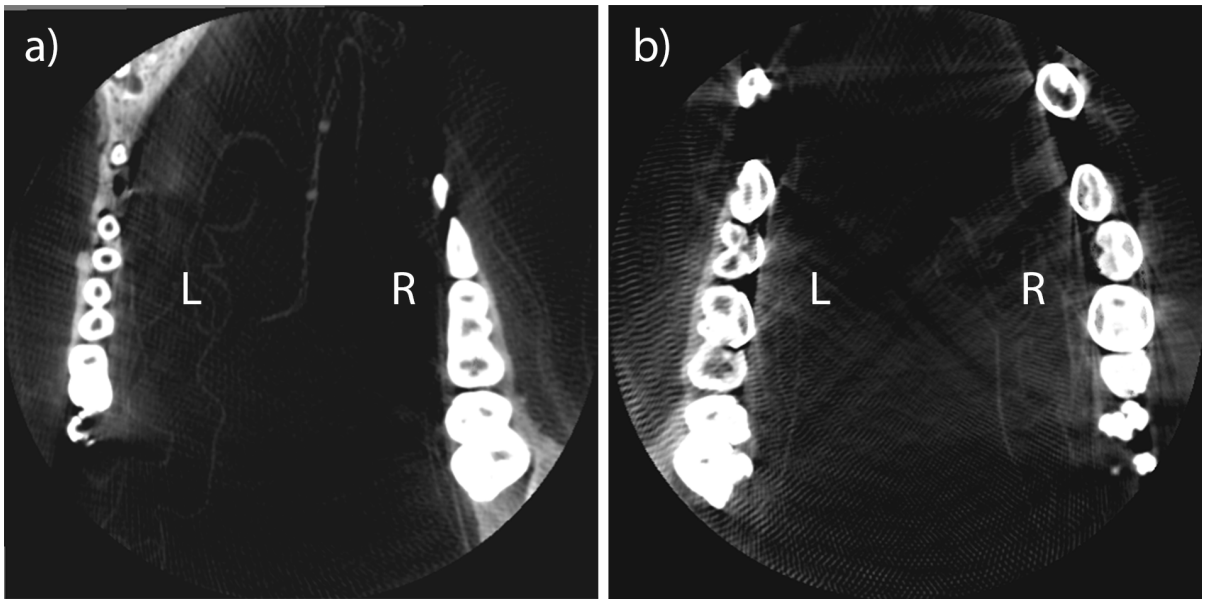

Figure 7. CBCT images from MicroView displaying the full arch FOV for Jaw B with (a) no restorations present, and (b) 8 SSCs present, with 4 SSCs on the left (L) side and 4 SSCs on the right (R) side.

3.2 Caliper and baseline CBCT measurements

The results of measurements with the caliper and baseline CBCT measurements for the full arch FOV with no restorations are listed in Table 1. When compared to the caliper measurements, the baseline measurements showed a variation range of 0.0 mm to 1.7 mm. In some cases, the baseline CBCT underestimated the caliper distance by up to 1.3 mm, while in others, the CBCT measurements showed an overestimation by up to 1.7 mm. The mean difference is 0.60 ± 0.41 mm.

	Jaw AA			Jaw BA			Jaw CA			Jaw A			Jaw B			Jaw C		
Gutta percha points	Caliper	CBCT	Diff	Caliper	CBCT	Diff	Caliper	CBCT	Diff	Caliper	CBCT	Diff	Caliper	CBCT	Diff	Caliper	CBCT	Diff
Left																		
GP-1 (mm)	5.0	5.6	0.6	5.2	5.1	-0.1	3.8	4.7	0.9	6.1	5.4	-0.7	6.1	6.9	0.8	4.1	5.8	1.7
GP-2 (mm)	7.5	7.3	-0.2	6.2	7.1	0.9	5.2	6.2	1.0	6.9	7.6	0.7	8.0	8.1	0.1	6.2	7.8	1.6
GP-3 (mm)	11.0	11.3	0.3	9.3	9.3	0.0	7.0	7.7	0.7	9.0	9.6	0.6	9.6	9.8	0.2	9.0	9.6	0.6
Right																		
GP-1 (mm)	5.2	5.8	0.6	4.4	4.3	-0.1	4.1	4.1	0.0	5.5	6.2	0.7	6.8	6.4	-0.4	5.4	4.7	-0.7
GP-2 (mm)	7.0	7.6	0.6	6.2	4.9	-1.3	5.8	6.6	0.8	7.3	6.7	-0.6	8.2	8.1	-0.2	7.5	7.2	-0.3
GP-3 (mm)	10.6	10.7	0.1	8.5	7.5	-1.0	6.9	7.5	0.6	8.5	9.0	0.5	9.1	9.8	0.7	9.3	10.0	0.7

Table 1. Caliper and baseline CBCT measurements for the full arch FOV, in mm, prior to any restorations being added.

3.3 Increasing number of restorations for full arch FOV and single site FOV

3.3.1 Amalgam restorations

The addition of amalgam restorations scanned as a full arch FOV produced a difference ranging from 0.11 ± 0.15 mm to 0.54 ± 0.64 mm when compared to scans taken at baseline with no restorations. The raw distances subtracted from the baseline measurements with no restorations answer the question of whether there is a difference in accuracy as the metal restorations increase. These results are shown in Table 2. As the number of restorations increased, no statistical difference was detected compared the baseline scan ($p>0.05$). There was also no trend found for this variation with the number of restorations added. The results were similar when scanned as a single site FOV, with the difference from the baseline scans ranging from 0.14 ± 0.16 mm to 0.40 ± 0.41 mm as shown in Table 3. Again, there was no statistically significant difference between the number of restoration groups ($p>0.05$) and no trend for the differences with the increasing number of restorations.

Comparing the distances to caliper measurements showed an increased range of differences, however, still no trend with number of restorations. The raw distances were subtracted from the caliper measurements directly, to answer the question of variation from caliper measurements as metal restorations increase. As shown in Table 4, the difference range from caliper measurements was 0.43 ± 0.45 mm to 1.18 ± 0.67 mm for the full arch FOV. When single site FOVs were taken, that difference ranged from 0.64 ± 0.46 mm to 1.01 ± 0.96 mm, and this is displayed in Table 5. No statistically significant difference was found between the groups of restorations ($p>0.05$).

.

	Jaw AA			Jaw BA			Jaw CA			Average		
# of Amg	MicroView	DTX	Carestream	MicroView	DTX	Carestream	MicroView	DTX	Carestream	MicroView	DTX	Carestream
Left : 1	0.53 ± 0.58	0.32 ± 0.42	0.12 ± 0.15	0.54 ± 0.50	0.52 ± 0.64	0.08 ± 0.10	0.16 ± 0.12	0.25 ± 0.31	0.13 ± 0.20	**0.41 ± 0.40**	**0.36 ± 0.46**	**0.11 ± 0.15**
Left : 2	0.28 ± 0.27	0.37 ± 0.45	0.20 ± 0.31	0.37 ± 0.44	0.33 ± 0.52	0.17 ± 0.23	0.20 ± 0.17	0.18 ± 0.26	0.20 ± 0.28	**0.28 ± 0.29**	**0.29 ± 0.41**	**0.19 ± 0.27**
Left : 3	0.27 ± 0.16	0.08 ± 0.14	0.10 ± 0.15	0.30 ± 0.36	0.53 ± 0.73	0.32 ± 0.17	0.33 ± 0.09	0.33 ± 0.41	0.17 ± 0.23	**0.30 ± 0.20**	**0.31 ± 0.43**	**0.20 ± 0.18**
Left : 4	0.30 ± 0.38	0.23 ± 0.24	0.17 ± 0.20	0.42 ± 0.46	0.53 ± 0.72	0.33 ± 0.36	0.39 ± 0.27	0.32 ± 0.39	0.17 ± 0.29	**0.37 ± 0.37**	**0.36 ± 0.45**	**0.22 ± 0.28**
Right : 5	0.33 ± 0.42	0.45 ± 0.60	0.17 ± 0.31	0.43 ± 0.48	0.43 ± 0.64	0.22 ± 0.31	0.19 ± 0.14	0.25 ± 0.31	0.13 ± 0.20	**0.32 ± 0.35**	**0.38 ± 0.52**	**0.17 ± 0.27**
Right: 6	0.50 ± 0.53	0.22 ± 0.34	0.48 ± 0.69	0.32 ± 0.47	0.50 ± 0.72	0.30 ± 0.36	0.26 ± 0.19	0.35 ± 0.38	0.30 ± 0.26	**0.36 ± 0.40**	**0.36 ± 0.48**	**0.36 ± 0.44**
Right: 7	0.28 ± 0.32	0.25 ± 0.26	0.25 ± 0.43	0.19 ± 0.16	0.50 ± 0.70	0.30 ± 0.52	1.14 ± 1.43	0.20 ± 0.29	0.13 ± 0.10	**0.54 ± 0.64**	**0.32 ± 0.42**	**0.23 ± 0.35**
Right: 8	0.40 ± 0.34	0.15 ± 0.21	0.30 ± 0.25	0.38 ± 0.26	0.50 ± 0.69	0.37 ± 0.55	0.31 ± 0.19	0.30 ± 0.39	0.28 ± 0.21	**0.36 ± 0.26**	**0.32 ± 0.43**	**0.32 ± 0.34**

Table 2. Amalgam full arch FOV (10x5 cm) group. The difference in mm, between distances measured on CBCT images with increasing restorations, and distances measured on baseline CBCT images with no restorations. Each difference shown is an average of three measurements (GP-1, GP-2, GP-3), and displayed as average ± standard deviation.

	Jaw AA			Jaw BA			Jaw CA			Average		
# of Amg	MicroView	DTX	Carestream	MicroView	DTX	Carestream	MicroView	DTX	Carestream	MicroView	DTX	Carestream
Left : 1	0.44 ± 0.59	0.17 ± 0.15	0.10 ± 0.00	0.11 ± 0.17	0.43 ± 0.50	0.27 ± 0.36	0.31 ± 0.36	0.33 ± 0.25	0.40 ± 0.44	**0.29 ± 0.37**	**0.31 ± 0.30**	**0.26 ± 0.27**
Left : 2	0.17 ± 0.18	0.10 ± 0.10	0.27 ± 0.31	0.31 ± 0.33	0.33 ± 0.32	0.10 ± 0.10	0.17 ± 0.22	0.23 ± 0.32	0.13 ± 0.15	**0.22 ± 0.24**	**0.22 ± 0.25**	**0.17 ± 0.19**
Left : 3	0.31 ± 0.19	0.43 ± 0.64	0.23 ± 0.35	0.15 ± 0.21	0.37 ± 0.57	0.10 ± 0.12	0.21 ± 0.21	0.30 ± 0.35	0.10 ± 0.10	**0.22 ± 0.20**	**0.37 ± 0.52**	**0.14 ± 0.19**
Left : 4	0.33 ± 0.54	0.10 ± 0.17	0.10 ± 0.12	0.56 ± 0.61	0.27 ± 0.31	0.10 ± 0.15	0.21 ± 0.16	0.27 ± 0.30	0.10 ± 0.12	**0.37 ± 0.44**	**0.21 ± 0.26**	**0.10 ± 0.13**
Right : 5	0.28 ± 0.35	0.37 ± 0.25	0.57 ± 0.60	0.29 ± 0.37	0.40 ± 0.50	0.13 ± 0.15	0.06 ± 0.07	0.20 ± 0.25	0.10 ± 0.12	**0.21 ± 0.26**	**0.32 ± 0.33**	**0.27 ± 0.29**
Right: 6	0.03 ± 0.04	0.30 ± 0.30	0.23 ± 0.26	0.27 ± 0.31	0.40 ± 0.55	0.10 ± 0.10	0.12 ± 0.14	0.23 ± 0.37	0.30 ± 0.31	**0.14 ± 0.16**	**0.31 ± 0.41**	**0.21 ± 0.22**
Right: 7	0.45 ± 0.65	0.47 ± 0.47	0.54 ± 0.75	0.34 ± 0.33	0.33 ± 0.51	0.17 ± 0.12	0.16 ± 0.21	0.40 ± 0.26	0.20 ± 0.21	**0.32 ± 0.40**	**0.40 ± 0.41**	**0.30 ± 0.36**
Right: 8	0.40 ± 0.04	0.13 ± 0.15	0.20 ± 0.21	0.41 ± 0.44	0.33 ± 0.47	0.27 ± 0.29	0.23 ± 0.24	0.37 ± 0.06	0.20 ± 0.25	**0.35 ± 0.24**	**0.28 ± 0.23**	**0.22 ± 0.25**

Table 3. Amalgam single site FOV (5x5 cm) group. The difference in mm, between distances measured on CBCT images with increasing restorations, and distances measured on baseline CBCT images with no restorations. Each difference shown is an average of three measurements (GP-1, GP-2, GP-3), and displayed as average ± standard deviation.

	Jaw AA				Jaw BA				Jaw CA				Average			
# of Amg	Semi-Automated MicroView	Manual MicroView	Manual DTX	Manual CS9300	Semi-Automated MicroView	Manual MicroView	Manual DTX	Manual CS9300	Semi-Automated MicroView	Manual MicroView	Manual DTX	Manual CS9300	Semi-Automated MicroView	Manual MicroView	Manual DTX	Manual CS9300
None	0.44 ± 0.49	0.37 ± 0.32	1.23 ± 0.54	1.13 ± 0.47	0.96 ± 1.19	0.56 ± 0.77	0.85 ± 0.77	1.07 ± 1.01	0.52 ± 0.59	0.67 ± 0.38	1.07 ± 0.51	0.90 ± 0.24	**0.64 ± 0.76**	**0.53 ± 0.49**	**1.05 ± 0.61**	**1.03 ± 0.57**
Left : 1	0.59 ± 0.68	0.76 ± 0.71	1.12 ± 0.45	1.12 ± 0.46	0.66 ± 0.92	0.79 ± 1.09	1.00 ± 1.13	1.05 ± 1.03	0.42 ± 0.48	0.53 ± 0.38	1.15 ± 0.55	0.90 ± 0.35	**0.56 ± 0.69**	**0.69 ± 0.73**	**1.09 ± 0.71**	**1.02 ± 0.61**
Left : 2	0.52 ± 0.68	0.56 ± 0.49	1.40 ± 0.64	1.10 ± 0.38	1.20 ± 1.03	0.30 ± 0.40	1.02 ± 1.08	1.03 ± 1.02	0.83 ± 0.92	0.61 ± 0.46	0.98 ± 0.45	1.00 ± 0.43	**0.85 ± 0.88**	**0.49 ± 0.45**	**1.13 ± 0.72**	**1.04 ± 0.61**
Left : 3	0.29 ± 0.39	0.58 ± 0.34	1.18 ± 0.48	1.10 ± 0.43	0.95 ± 1.09	0.47 ± 0.59	1.02 ± 1.17	1.08 ± 1.15	0.55 ± 0.65	0.43 ± 0.35	1.00 ± 0.50	1.03 ± 0.37	**0.60 ± 0.71**	**0.49 ± 0.43**	**1.07 ± 0.72**	**1.07 ± 0.65**
Left : 4	0.49 ± 0.40	0.63 ± 0.60	1.03 ± 0.55	1.07 ± 0.49	0.96 ± 1.07	0.31 ± 0.39	1.02 ± 1.16	0.93 ± 1.05	0.39 ± 0.46	0.35 ± 0.35	0.98 ± 0.42	0.93 ± 0.43	**0.61 ± 0.64**	**0.43 ± 0.45**	**1.01 ± 0.71**	**0.98 ± 0.66**
Right : 5	0.75 ± 0.87	0.53 ± 0.58	1.25 ± 0.85	1.23 ± 0.27	1.11 ± 1.29	0.43 ± 0.54	0.92 ± 1.05	0.95 ± 0.96	0.47 ± 0.55	0.57 ± 0.43	1.15 ± 0.55	0.90 ± 0.35	**0.78 ± 0.90**	**0.51 ± 0.52**	**1.11 ± 0.82**	**1.03 ± 0.53**
Right: 6	0.98 ± 1.25	0.80 ± 0.69	1.28 ± 0.35	1.45 ± 0.37	1.04 ± 1.13	0.33 ± 0.43	0.95 ± 1.09	0.90 ± 1.00	0.46 ± 0.54	0.48 ± 0.36	1.15 ± 0.48	1.17 ± 0.43	**0.83 ± 0.97**	**0.54 ± 0.49**	**1.13 ± 0.64**	**1.17 ± 0.60**
Right: 7	0.80 ± 0.89	0.58 ± 0.50	1.12 ± 0.58	1.38 ± 0.67	0.96 ± 1.00	0.47 ± 0.66	0.98 ± 1.13	0.93 ± 1.07	1.00 ± 1.64	0.95 ± 1.26	1.10 ± 0.28	1.03 ± 0.31	**0.92 ± 1.18**	**0.67 ± 0.81**	**1.07 ± 0.66**	**1.11 ± 0.68**
Right: 8	1.09 ± 1.52	0.63 ± 0.40	1.22 ± 0.57	1.43 ± 0.59	1.03 ± 1.12	0.31 ± 0.38	0.98 ± 0.99	1.00 ± 0.93	0.55 ± 0.65	0.46 ± 0.45	1.10 ± 0.60	1.12 ± 0.48	**0.89 ± 1.10**	**0.47 ± 0.41**	**1.10 ± 0.72**	**1.18 ± 0.67**

Table 4. Amalgam full arch FOV (10x5 cm) group. The difference in mm, between distances measured on CBCT images, and distances measured with the digital caliper. Each difference shown is an average of three measurements (GP-1, GP-2, GP-3), and displayed as average ± standard deviation.

	Jaw AA				Jaw BA				Jaw CA				Average			
# of Amg	Semi-Automated MicroView	Manual MicroView	Manual DTX	Manual CS9300	Semi-Automated MicroView	Manual MicroView	Manual DTX	Manual CS9300	Semi-Automated MicroView	Manual MicroView	Manual DTX	Manual CS9300	Semi-Automated MicroView	Manual MicroView	Manual DTX	Manual CS9300
None	0.55 ± 0.71	0.54 ± 0.53	0.73 ± 0.64	0.77 ± 0.59	1.42 ± 1.73	1.13 ± 0.51	0.87 ± 0.90	0.83 ± 0.40	0.29 ± 0.42	0.53 ± 0.62	0.43 ± 0.32	0.57 ± 0.57	**0.75 ± 0.95**	**0.73 ± 0.55**	**0.68 ± 0.62**	**0.72 ± 0.52**
Left : 1	0.44 ± 0.49	0.54 ± 0.87	0.77 ± 0.75	0.87 ± 0.59	1.70 ± 1.48	1.12 ± 0.39	1.10 ± 0.40	1.03 ± 0.68	0.52 ± 0.30	0.57 ± 0.57	0.77 ± 0.23	0.77 ± 0.23	**0.89 ± 0.76**	**0.74 ± 0.61**	**0.88 ± 0.46**	**0.89 ± 0.50**
Left : 2	0.40 ± 0.44	0.71 ± 0.71	0.77 ± 0.72	0.70 ± 0.67	1.82 ± 1.30	0.91 ± 0.36	1.13 ± 0.60	0.73 ± 0.35	0.30 ± 0.39	0.48 ± 0.45	0.67 ± 0.64	0.50 ± 0.52	**0.84 ± 0.71**	**0.70 ± 0.51**	**0.86 ± 0.65**	**0.64 ± 0.51**
Left : 3	0.43 ± 0.59	0.75 ± 0.42	0.57 ± 0.46	0.73 ± 0.60	1.92 ± 1.37	1.04 ± 0.34	1.03 ± 0.40	0.87 ± 0.40	0.36 ± 0.36	0.39 ± 0.50	0.73 ± 0.67	0.67 ± 0.55	**0.90 ± 0.77**	**0.73 ± 0.42**	**0.78 ± 0.51**	**0.76 ± 0.52**
Left : 4	0.51 ± 0.65	0.38 ± 0.60	0.63 ± 0.55	0.73 ± 0.64	1.67 ± 1.39	0.65 ± 0.37	1.00 ± 0.60	0.87 ± 0.55	0.29 ± 0.39	0.39 ± 0.64	0.63 ± 0.59	0.60 ± 0.61	**0.82 ± 0.81**	**0.47 ± 0.54**	**0.75 ± 0.58**	**0.73 ± 0.60**
Right : 5	0.54 ± 0.22	0.57 ± 0.53	1.10 ± 0.50	1.27 ± 0.40	1.79 ± 1.42	1.06 ± 0.39	1.07 ± 0.40	0.77 ± 0.31	0.29 ± 0.41	0.49 ± 0.67	0.57 ± 0.55	0.60 ± 0.46	**0.87 ± 0.68**	**0.71 ± 0.53**	**0.91 ± 0.48**	**0.88 ± 0.39**
Right: 6	0.43 ± 0.67	0.55 ± 0.52	0.63 ± 0.67	0.73 ± 0.68	1.62 ± 1.42	0.90 ± 0.30	1.00 ± 0.36	0.93 ± 0.45	0.71 ± 0.77	0.47 ± 0.57	0.60 ± 0.70	0.80 ± 0.78	**0.92 ± 0.95**	**0.64 ± 0.46**	**0.74 ± 0.58**	**0.82 ± 0.64**
Right: 7	1.00 ± 0.95	0.96 ± 1.17	0.93 ± 1.10	1.17 ± 1.33	1.70 ± 1.44	0.89 ± 0.48	1.00 ± 0.44	1.00 ± 0.30	0.32 ± 0.49	0.53 ± 0.51	0.83 ± 0.51	0.70 ± 0.61	**1.01 ± 0.96**	**0.79 ± 0.72**	**0.92 ± 0.68**	**0.96 ± 0.75**
Right: 8	0.62 ± 0.65	0.84 ± 0.54	0.87 ± 0.78	0.90 ± 0.60	1.55 ± 1.39	0.86 ± 0.40	0.93 ± 0.49	0.97 ± 0.46	0.39 ± 0.44	0.42 ± 0.62	0.20 ± 0.31	0.63 ± 0.59	**0.85 ± 0.83**	**0.71 ± 0.52**	**0.67 ± 0.53**	**0.83 ± 0.55**

Table 5. Amalgam single site FOV (5x5 cm) group. The difference in mm, between distances measured on CBCT images, and distances measured with the digital caliper. Each difference shown is an average of three measurements (GP-1, GP-2, GP-3), and displayed as average ± standard deviation.

3.3.2 Stainless steel crown restorations

The addition of SSC restorations scanned as a full arch FOV resulted in differences ranging from 0.21 ± 0.26 mm to 0.60 ± 0.60 mm when compared to baseline scans. These results are displayed in Table 6. No statistically significant difference was found between the measurements made at any number of added restorations compared to baseline scans with no restorations ($p>0.05$). No trend was shown for these differences with the number of restorations.

For the single site FOV, the range of differences was from 0.21 ± 0.22 mm to 0.62 ± 0.64 mm and the results are shown in Table 7. There was also no statistical difference between the restoration groups ($p>0.05$) and no trend for the differences.

Comparing the results to caliper measurements showed an increased range of differences than when they were compared to baseline measurements. For the full arch FOV shown in Table 8, the differences range from 0.61 ± 0.73 mm to 0.88 ± 0.43 mm. The results are similar for the single site FOV shown in Table 9, with difference ranging from 0.40 ± 0.66 mm to 0.97 ± 0.74 mm. No statistically significant difference was found between the groups of restorations ($p>0.05$).

Figure 8 is a graph showing the difference between group means (with increasing number of restorations, 1-8) compared to the control group mean with no restorations. Figure 8 (a) shows that amalgam restorations in the full arch FOV had larger confidence intervals compared to the other groups (amalgam restorations in the single site FOV, and SSC restorations in the full arch or single site FOV). The larger confidence intervals point to a greater heterogeneity in the data. Table 10 is the corresponding ANOVA table showing p-values for each restoration type and FOV.

	Jaw A			Jaw B			Jaw C			Average		
# of SSC	MicroView	DTX	Carestream	MicroView	DTX	Carestream	MicroView	DTX	Carestream	MicroView	DTX	Carestream
Left : 1	0.37 ± 0.58	0.35 ± 0.43	0.30 ± 0.40	0.17 ± 0.20	0.52 ± 0.59	0.10 ± 0.11	0.38 ± 0.55	0.47 ± 0.56	0.90 ± 1.11	**0.31 ± 0.44**	**0.45 ± 0.53**	**0.43 ± 0.54**
Left : 2	0.39 ± 0.55	0.42 ± 0.49	0.70 ± 0.57	0.16 ± 0.14	0.43 ± 0.54	0.22 ± 0.12	0.29 ± 0.50	0.48 ± 0.61	0.88 ± 1.10	**0.28 ± 0.40**	**0.44 ± 0.55**	**0.60 ± 0.60**
Left : 3	0.38 ± 0.51	0.37 ± 0.52	0.38 ± 0.52	0.31 ± 0.19	0.48 ± 0.61	0.38 ± 0.25	0.25 ± 0.26	0.62 ± 0.66	0.80 ± 1.00	**0.31 ± 0.32**	**0.49 ± 0.60**	**0.52 ± 0.59**
Left : 4	0.42 ± 0.52	0.17 ± 0.21	0.58 ± 0.59	0.15 ± 0.11	0.23 ± 0.28	0.23 ± 0.15	0.32 ± 0.49	0.53 ± 0.60	0.78 ± 0.97	**0.30 ± 0.37**	**0.31 ± 0.36**	**0.53 ± 0.57**
Right : 5	0.62 ± 0.62	0.17 ± 0.21	0.45 ± 0.60	0.19 ± 0.18	0.25 ± 0.34	0.30 ± 0.17	0.18 ± 0.21	0.20 ± 0.22	0.12 ± 0.12	**0.33 ± 0.34**	**0.21 ± 0.26**	**0.29 ± 0.30**
Right: 6	0.34 ± 0.47	1.05 ± 0.57	0.50 ± 0.53	0.19 ± 0.20	0.20 ± 0.27	0.27 ± 0.31	0.39 ± 0.67	0.45 ± 0.53	0.17 ± 0.21	**0.31 ± 0.45**	**0.57 ± 0.46**	**0.31 ± 0.35**
Right: 7	0.41 ± 0.64	0.40 ± 0.24	0.42 ± 0.59	0.25 ± 0.33	0.27 ± 0.19	0.23 ± 0.25	0.23 ± 0.25	0.23 ± 0.27	0.15 ± 0.15	**0.30 ± 0.41**	**0.30 ± 0.23**	**0.27 ± 0.33**
Right: 8	0.36 ± 0.33	0.40 ± 0.26	0.53 ± 0.62	0.32 ± 0.42	0.32 ± 0.10	0.32 ± 0.29	0.30 ± 0.26	0.33 ± 0.40	0.18 ± 0.20	**0.33 ± 0.34**	**0.35 ± 0.25**	**0.34 ± 0.37**

Table 6. SSC full arch FOV (10x5 cm) group. The difference in mm, between distances measured on CBCT images with increasing restorations, and distances measured on baseline CBCT images with no restorations. Each difference shown is an average of three measurements (GP-1, GP-2, GP-3), and displayed as average ± standard deviation.

	Jaw A			Jaw B			Jaw C			Average		
# of SSC	MicroView	DTX	Carestream	MicroView	DTX	Carestream	MicroView	DTX	Carestream	MicroView	DTX	Carestream
Left : 1	0.73 ± 0.45	0.60 ± 0.62	0.63 ± 0.70	0.10 ± 0.11	0.13 ± 0.15	0.13 ± 0.06	0.79 ± 0.78	0.90 ± 0.97	0.70 ± 0.80	**0.54 ± 0.45**	**0.54 ± 0.58**	**0.49 ± 0.52**
Left : 2	0.53 ± 0.41	0.23 ± 0.15	0.43 ± 0.50	0.22 ± 0.30	0.23 ± 0.30	0.13 ± 0.15	0.76 ± 0.95	0.83 ± 0.81	0.37 ± 0.21	**0.50 ± 0.55**	**0.43 ± 0.42**	**0.31 ± 0.29**
Left : 3	0.36 ± 0.28	0.43 ± 0.49	0.70 ± 0.75	0.19 ± 0.11	0.17 ± 0.21	0.23 ± 0.06	0.81 ± 0.85	0.83 ± 1.00	0.87 ± 1.01	**0.45 ± 0.41**	**0.48 ± 0.57**	**0.60 ± 0.61**
Left : 4	0.47 ± 0.30	0.50 ± 0.53	0.67 ± 0.74	0.24 ± 0.07	0.07 ± 0.12	0.27 ± 0.12	0.69 ± 0.93	0.73 ± 0.85	0.93 ± 1.07	**0.47 ± 0.43**	**0.43 ± 0.50**	**0.62 ± 0.64**
Right : 5	0.40 ± 0.50	0.20 ± 0.21	0.33 ± 0.31	0.20 ± 0.12	0.37 ± 0.15	0.07 ± 0.06	0.13 ± 0.18	0.17 ± 0.21	0.37 ± 0.06	**0.24 ± 0.27**	**0.25 ± 0.19**	**0.26 ± 0.14**
Right: 6	0.43 ± 0.47	0.33 ± 0.31	0.37 ± 0.31	0.17 ± 0.10	0.07 ± 0.12	0.23 ± 0.06	0.14 ± 0.16	0.20 ± 0.32	0.40 ± 0.00	**0.25 ± 0.24**	**0.20 ± 0.25**	**0.33 ± 0.12**
Right: 7	0.32 ± 0.40	0.37 ± 0.25	0.47 ± 0.46	0.08 ± 0.11	0.17 ± 0.26	0.10 ± 0.00	0.23 ± 0.14	0.20 ± 0.26	0.53 ± 0.21	**0.21 ± 0.22**	**0.25 ± 0.26**	**0.37 ± 0.22**
Right: 8	0.34 ± 0.41	0.43 ± 0.55	0.33 ± 0.31	0.07 ± 0.07	0.40 ± 0.26	0.13 ± 0.21	0.25 ± 0.36	0.13 ± 0.15	0.40 ± 0.20	**0.22 ± 0.28**	**0.32 ± 0.32**	**0.29 ± 0.24**

Table 7. SSC single site FOV (5x5 cm) group. The difference in mm, between distances measured on CBCT images with increasing restorations, and distances measured on baseline CBCT images with no restorations. Each difference shown is an average of three measurements (GP-1, GP-2, GP-3), and displayed as average ± standard deviation.

	Jaw A				Jaw B				Jaw C				Average			
# of SSC	Semi-Automated MicroView	Manual MicroView	Manual DTX	Manual CS9300	Semi-Automated MicroView	Manual MicroView	Manual DTX	Manual CS9300	Semi-Automated MicroView	Manual MicroView	Manual DTX	Manual CS9300	Semi-Automated MicroView	Manual MicroView	Manual DTX	Manual CS9300
None	0.81 ± 0.57	0.61 ± 0.65	0.65 ± 0.39	0.68 ± 0.58	0.43 ± 0.52	0.38 ± 0.47	0.43 ± 0.36	0.58 ± 0.21	1.00 ± 1.25	0.94 ± 0.97	1.10 ± 0.30	1.07 ± 1.06	**0.75 ± 0.78**	**0.64 ± 0.70**	**0.73 ± 0.35**	**0.78 ± 0.62**
Left : 1	0.83 ± 0.57	0.73 ± 0.82	0.70 ± 0.63	0.65 ± 0.59	0.39 ± 0.48	0.46 ± 0.57	0.32 ± 0.33	0.48 ± 0.21	0.77 ± 1.02	0.87 ± 1.07	0.90 ± 0.39	1.03 ± 0.25	**0.66 ± 0.69**	**0.69 ± 0.82**	**0.64 ± 0.45**	**0.72 ± 0.35**
Left : 2	0.85 ± 0.56	0.61 ± 0.73	0.77 ± 0.68	1.12 ± 0.73	0.47 ± 0.58	0.37 ± 0.49	0.50 ± 0.35	0.37 ± 0.18	1.20 ± 1.52	0.85 ± 0.98	0.88 ± 0.48	0.85 ± 0.15	**0.84 ± 0.89**	**0.61 ± 0.73**	**0.72 ± 0.50**	**0.78 ± 0.35**
Left : 3	0.88 ± 0.69	0.61 ± 0.70	0.88 ± 0.73	0.67 ± 0.62	0.48 ± 0.59	0.49 ± 0.58	0.35 ± 0.40	0.23 ± 0.18	1.00 ± 1.30	0.81 ± 0.98	0.68 ± 0.63	0.87 ± 0.27	**0.79 ± 0.86**	**0.64 ± 0.75**	**0.64 ± 0.59**	**0.59 ± 0.36**
Left : 4	0.88 ± 0.55	0.57 ± 0.63	0.58 ± 0.57	0.97 ± 0.61	0.53 ± 0.61	0.42 ± 0.52	0.57 ± 0.31	0.35 ± 0.24	0.78 ± 1.04	0.86 ± 1.10	0.87 ± 0.46	0.95 ± 0.35	**0.73 ± 0.73**	**0.62 ± 0.75**	**0.67 ± 0.45**	**0.76 ± 0.40**
Right : 5	0.82 ± 0.58	0.98 ± 0.98	0.82 ± 0.57	0.63 ± 0.50	0.51 ± 0.59	0.46 ± 0.54	0.42 ± 0.29	0.32 ± 0.35	0.98 ± 1.24	0.76 ± 0.90	0.97 ± 0.24	1.02 ± 1.04	**0.77 ± 0.80**	**0.73 ± 0.81**	**0.74 ± 0.37**	**0.66 ± 0.63**
Right: 6	0.66 ± 0.62	0.61 ± 0.68	1.35 ± 0.74	0.82 ± 0.58	0.42 ± 0.52	0.41 ± 0.49	0.40 ± 0.23	0.45 ± 0.44	1.20 ± 1.50	0.98 ± 1.11	0.88 ± 0.32	1.00 ± 0.98	**0.76 ± 0.88**	**0.67 ± 0.76**	**0.88 ± 0.43**	**0.76 ± 0.67**
Right: 7	0.67 ± 0.58	0.67 ± 0.86	1.05 ± 0.62	0.60 ± 0.52	0.42 ± 0.51	0.57 ± 0.67	0.27 ± 0.33	0.42 ± 0.29	0.89 ± 1.09	0.83 ± 1.04	1.07 ± 0.12	0.95 ± 1.06	**0.66 ± 0.73**	**0.69 ± 0.86**	**0.80 ± 0.36**	**0.66 ± 0.62**
Right: 8	1.21 ± 0.86	0.63 ± 0.58	1.05 ± 0.49	0.78 ± 0.51	0.40 ± 0.55	0.65 ± 0.76	0.28 ± 0.33	0.40 ± 0.29	1.00 ± 1.29	0.70 ± 0.90	1.00 ± 0.27	1.12 ± 1.08	**0.87 ± 0.90**	**0.66 ± 0.75**	**0.78 ± 0.36**	**0.77 ± 0.63**

Table 8. SSC full arch FOV (10x5 cm) group. The difference in mm, between distances measured on CBCT images, and distances measured with the digital caliper. Each difference shown is an average of three measurements (GP-1, GP-2, GP-3), and displayed as average ± standard deviation.

	Jaw A				Jaw B				Jaw C				Average			
# of SSC	Semi-Automated MicroView	Manual MicroView	Manual DTX	Manual CS9300	Semi-Automated MicroView	Manual MicroView	Manual DTX	Manual CS9300	Semi-Automated MicroView	Manual MicroView	Manual DTX	Manual CS9300	Semi-Automated MicroView	Manual MicroView	Manual DTX	Manual CS9300
None	0.75 ± 0.59	0.23 ± 0.73	0.23 ± 0.87	0.20 ± 0.76	0.39 ± 0.61	0.48 ± 0.64	0.60 ± 0.72	0.53 ± 0.67	0.30 ± 0.43	0.49 ± 0.62	0.43 ± 0.42	0.57 ± 0.25	**0.48 ± 0.54**	**0.40 ± 0.66**	**0.42 ± 0.67**	**0.43 ± 0.56**
Left : 1	1.20 ± 0.50	0.70 ± 0.43	0.70 ± 0.38	0.63 ± 0.58	0.36 ± 0.37	0.42 ± 0.41	0.43 ± 0.50	0.57 ± 0.38	0.26 ± 0.17	0.41 ± 0.31	0.70 ± 0.17	1.50 ± 0.78	**0.61 ± 0.35**	**0.51 ± 0.38**	**0.61 ± 0.35**	**0.90 ± 0.58**
Left : 2	0.95 ± 0.40	0.50 ± 0.56	0.40 ± 0.76	0.43 ± 0.81	0.70 ± 0.95	0.51 ± 0.32	0.33 ± 0.58	0.37 ± 0.40	0.77 ± 0.29	0.83 ± 0.33	0.50 ± 0.17	0.70 ± 0.10	**0.81 ± 0.55**	**0.61 ± 0.40**	**0.41 ± 0.50**	**0.50 ± 0.44**
Left : 3	1.14 ± 0.40	0.34 ± 0.58	0.53 ± 0.78	0.77 ± 0.84	0.40 ± 0.61	0.30 ± 0.32	0.27 ± 0.38	0.67 ± 0.38	0.75 ± 0.26	0.65 ± 0.10	0.70 ± 0.40	1.47 ± 1.01	**0.76 ± 0.42**	**0.43 ± 0.33**	**0.50 ± 0.52**	**0.97 ± 0.74**
Left : 4	1.19 ± 0.41	0.49 ± 0.48	0.60 ± 0.50	0.73 ± 0.53	0.77 ± 0.41	0.43 ± 0.37	0.37 ± 0.38	0.23 ± 0.38	0.82 ± 0.44	0.80 ± 0.48	0.73 ± 0.32	1.53 ± 1.07	**0.93 ± 0.42**	**0.57 ± 0.44**	**0.57 ± 0.40**	**0.83 ± 0.66**
Right : 5	0.57 ± 0.47	0.47 ± 0.56	0.43 ± 0.55	0.53 ± 0.50	0.48 ± 0.37	0.29 ± 0.31	0.13 ± 0.21	0.50 ± 0.36	1.76 ± 1.12	1.18 ± 0.91	1.43 ± 0.64	0.70 ± 0.26	**0.94 ± 0.65**	**0.65 ± 0.59**	**0.66 ± 0.47**	**0.58 ± 0.37**
Right: 6	0.50 ± 0.66	0.50 ± 0.50	0.57 ± 0.49	0.50 ± 0.68	0.31 ± 0.34	0.32 ± 0.38	0.43 ± 0.45	0.27 ± 0.36	1.82 ± 1.12	1.23 ± 0.91	1.40 ± 1.11	0.67 ± 0.31	**0.88 ± 0.71**	**0.68 ± 0.60**	**0.80 ± 0.68**	**0.48 ± 0.45**
Right: 7	0.57 ± 0.37	0.39 ± 0.79	0.53 ± 0.81	0.67 ± 0.95	0.28 ± 0.37	0.44 ± 0.33	0.53 ± 0.59	0.33 ± 0.32	1.78 ± 1.12	1.39 ± 0.82	1.27 ± 1.12	0.53 ± 0.25	**0.88 ± 0.62**	**0.74 ± 0.65**	**0.78 ± 0.84**	**0.51 ± 0.51**
Right: 8	0.69 ± 1.26	0.41 ± 1.22	0.27 ± 0.70	0.53 ± 0.81	0.37 ± 0.61	0.41 ± 0.45	0.10 ± 0.12	0.50 ± 0.52	1.49 ± 0.93	1.30 ± 1.26	1.20 ± 0.87	0.67 ± 0.31	**0.85 ± 0.93**	**0.71 ± 0.98**	**0.52 ± 0.56**	**0.57 ± 0.55**

Table 9. SSC full arch FOV (10x5 cm) group. The difference in mm, between distances measured on CBCT images, and distances measured with the digital caliper. Each difference shown is an average of three measurements (GP-1, GP-2, GP-3), and displayed as average ± standard deviation.

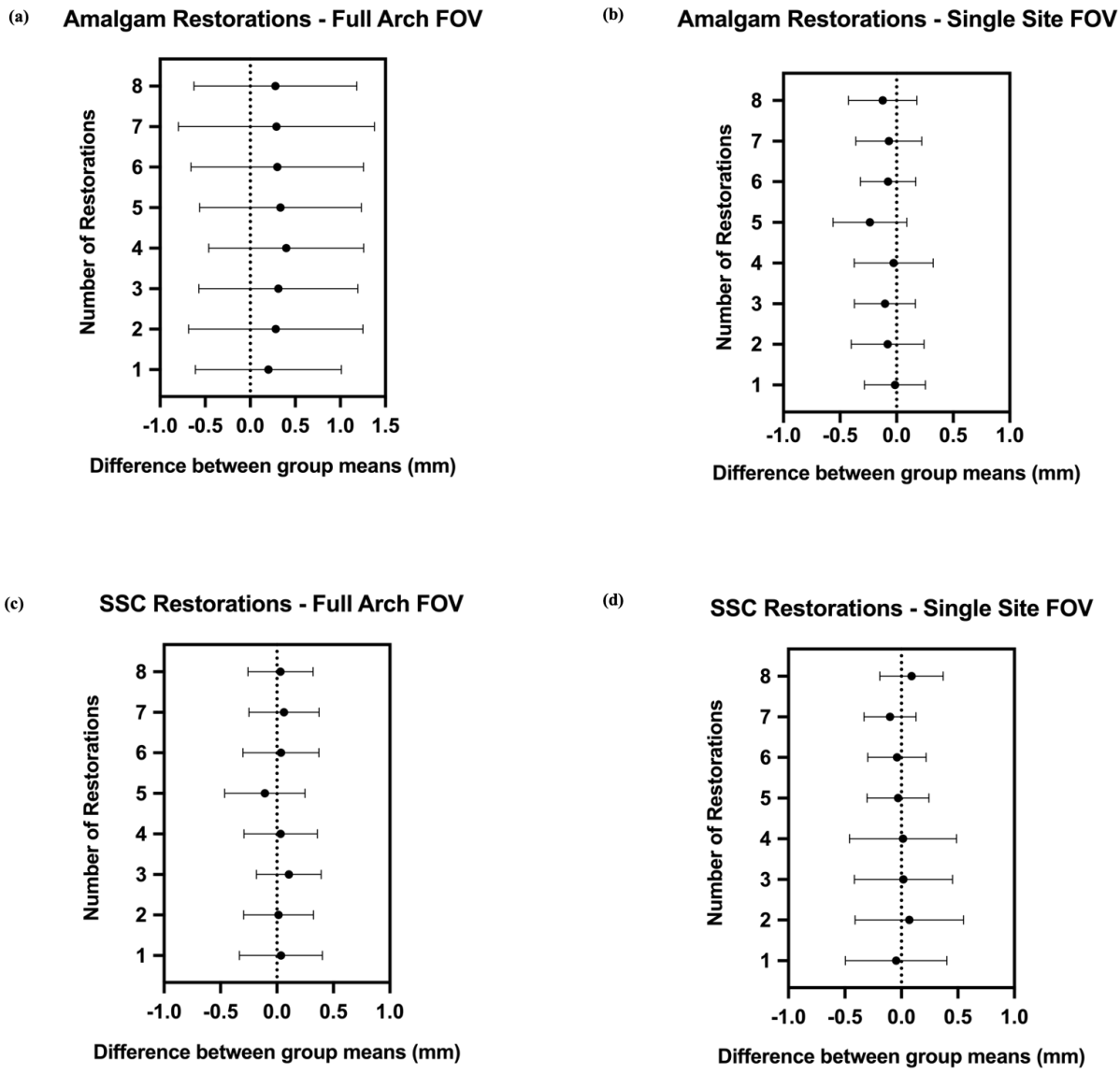

Figure 8. The difference between group means as the number of restorations increase compared to the control group with no restorations, measured in mm, with 95% confidence intervals.

ANOVA Table	SS	DF	MS	F (DFn, DFd)	P value
Amalgam – Full Arch FOV					
Treatment (between columns)	1.832	8	0.2290	F (2.612, 44.40) = 0.6642	P = 0.5584
Individual (between rows)	676.1	17	39.77	F (17, 136) = 115.3	P < 0.0001
Residual (random)	46.89	136	0.3448		
Total	724.9	161			
Amalgam – Single Site FOV					
Treatment (between columns)	0.7292	8	0.09115	F (5.333, 90.65) = 1.275	P = 0.2798
Individual (between rows)	698.8	17	41.11	F (17, 136) = 575.2	P < 0.0001
Residual (random)	9.719	136	0.07146		
Total	709.2	161			
SSC – Full Arch FOV					
Treatment (between columns)	0.4735	8	0.05918	F (4.415, 75.06) = 0.9629	P = 0.4389
Individual (between rows)	413.2	17	24.30	F (17, 136) = 395.4	P < 0.0001
Residual (random)	8.360	136	0.06147		
Total	422.0	161			
SSC – Single Site FOV					
Treatment (between columns)	0.5040	8	0.06300	F (2.038, 34.64) = 0.4197	P = 0.6643
Individual (between rows)	390.6	17	22.98	F (17, 136) = 153.1	P < 0.0001
Residual (random)	20.41	136	0.1501		
Total	411.6	161			

Table 10. ANOVA tables showing the P values for each restoration type in a full arch or single site FOV, comparing the control group of no restorations to increasing numbers of restorations.

3.4 Inside and outside the single site FOV

When comparing measurements with amalgam restorations inside the FOV to measurements with amalgam restorations outside the FOV, there was no significant difference compared to baseline measurements ($p>0.05$). These results are shown in Table 11. Similarly, no difference was found between the measurements taken with SSC restorations inside the FOV compared to outside the FOV ($p>0.05$). These results are shown in Table 12.

	MicroView		DTX		CS9300	
# of Amg	Inside FOV	Outside FOV	Inside FOV	Outside FOV	Inside FOV	Outside FOV
Left : 1	0.29 ± 0.37	0.24 ± 0.35	0.31 ± 0.30	0.37 ± 0.28	0.26 ± 0.27	0.29 ± 0.27
Left : 2	0.22 ± 0.24	0.43 ± 0.56	0.22 ± 0.25	0.26 ± 0.20	0.17 ± 0.19	0.26 ± 0.32
Left : 3	0.22 ± 0.20	0.34 ± 0.48	0.37 ± 0.52	0.24 ± 0.28	0.14 ± 0.19	0.23 ± 0.21
Left : 4	0.37 ± 0.44	0.25 ± 0.40	0.21 ± 0.26	0.21 ± 0.25	0.10 ± 0.13	0.19 ± 0.29
Right : 5	0.21 ± 0.26	0.52 ± 0.32	0.32 ± 0.33	0.18 ± 0.23	0.27 ± 0.29	0.27 ± 0.31
Right: 6	0.14 ± 0.16	0.28 ± 0.42	0.31 ± 0.41	0.28 ± 0.32	0.21 ± 0.22	0.25 ± 0.30
Right: 7	0.32 ± 0.40	0.26 ± 0.38	0.40 ± 0.41	0.25 ± 0.35	0.30 ± 0.36	0.23 ± 0.25
Right: 8	0.35 ± 0.24	0.33 ± 0.47	0.28 ± 0.23	0.27 ± 0.32	0.22 ± 0.25	0.28 ± 0.33

Table 11. Amalgam single site FOV (5x5 cm) inside and outside the FOV. The difference measured in mm, between distances measured on CBCT images with increasing restorations, and distances measured on baseline CBCT images with no restorations. Each difference shown is an average of three measurements (GP-1, GP-2, GP-3), and displayed as an average ± standard deviation.

	MicroView		DTX		CS9300	
# of SSC	Inside FOV	Outside FOV	Inside FOV	Outside FOV	Inside FOV	Outside FOV
Left : 1	0.54 ± 0.45	0.41 ± 0.44	0.54 ± 0.58	0.41 ± 0.42	0.49 ± 0.52	0.38 ± 0.34
Left : 2	0.50 ± 0.55	0.49 ± 0.65	0.43 ± 0.42	0.29 ± 0.29	0.31 ± 0.29	0.18 ± 0.07
Left : 3	0.45 ± 0.41	0.52 ± 0.50	0.48 ± 0.57	0.41 ± 0.44	0.60 ± 0.60	0.41 ± 0.31
Left : 4	0.41 ± 0.43	0.57 ± 0.63	0.43 ± 0.50	0.44 ± 0.49	0.62 ± 0.64	0.49 ± 0.48
Right : 5	0.24 ± 0.27	0.32 ± 0.29	0.25 ± 0.19	0.35 ± 0.43	0.26 ± 0.14	0.25 ± 0.32
Right: 6	0.25 ± 0.24	0.32 ± 0.27	0.20 ± 0.25	0.17 ± 0.20	0.33 ± 0.12	0.43 ± 0.34
Right: 7	0.21 ± 0.22	0.32 ± 0.20	0.25 ± 0.26	0.28 ± 0.41	0.37 ± 0.22	0.51 ± 0.49
Right: 8	0.22 ± 0.28	0.37 ± 0.33	0.32 ± 0.32	0.19 ± 0.26	0.29 ± 0.24	0.49 ± 0.43

Table 12. SSC single site FOV (5x5 cm) inside and outside the FOV. The difference measured in mm, between distances measured on CBCT images with increasing restorations, and distances measured on baseline CBCT images with no restorations. Each difference shown is an average of three measurements (GP-1, GP-2, GP-3), and displayed as an average ± standard deviation.

3.5 Altered CBCT scanning protocols

Measurement differences with increasing SSC restorations (1-8 SSCs) were subtracted from baseline CBCT measurements. These differences were averaged for three jaws with unchanged scan protocols (Jaw A, B, and C) and compared with differences for jaws with altered scan protocols (Jaw D, E, and F).

3.5.1 Increased peak kilovoltage

Table 13 shows the results when the peak kilovoltage of the scans was 84 kVp and increased to 90 kVp. When compared to baseline CBCT measurements, the differences ranged from 0.01 ± 0.14 mm to 0.44 ± 0.61 mm at the lower kVp. Meanwhile, at the higher kVp, the differences ranged from 0.00 ± 0.16 mm to 0.24 ± 0.31 mm. The increase in kVp did not result in measurements that were statistically significant ($p>0.05$). The measurements were also not

significantly different with increasing numbers of restorations, or when measured manually in three software packages (DTX, CS9300, and MicroView) ($p>0.05$ for all comparisons).

	Low KVP (84)			High KVP (90)		
# of SSC	MicroView	DTX	Carestream	MicroView	DTX	Carestream
Left : 1	0.03 ± 0.45	0.01 ± 0.58	0.38 ± 0.52	0.15 ± 0.22	0.01 ± 0.22	0.10 ± 0.15
Left : 2	0.07 ± 0.55	0.21 ± 0.42	0.04 ± 0.29	0.02 ± 0.21	0.09 ± 0.21	0.04 ± 0.19
Left : 3	0.11 ± 0.41	0.10 ± 0.57	0.44 ± 0.61	0.00 ± 0.09	0.09 ± 0.09	0.01 ± 0.27
Left : 4	0.02 ± 0.43	0.03 ± 0.50	0.29 ± 0.64	0.08 ± 0.31	0.24 ± 0.31	0.12 ± 0.18
Right : 5	0.05 ± 0.27	0.14 ± 0.19	0.01 ± 0.14	0.00 ± 0.16	0.06 ± 0.16	0.14 ± 0.20
Right: 6	0.06 ± 0.25	0.13 ± 0.25	0.09 ± 0.12	0.12 ± 0.21	0.10 ± 0.21	0.06 ± 0.19
Right: 7	0.09 ± 0.22	0.16 ± 0.26	0.08 ± 0.22	0.01 ± 0.24	0.19 ± 0.24	0.14 ± 0.27
Right: 8	0.15 ± 0.28	0.10 ± 0.32	0.00 ± 0.24	0.00 ± 0.28	0.14 ± 0.28	0.08 ± 0.18

Table 13. Altered kVp groups. The difference in mm, between distances measured on CBCT images with increasing number of restorations, and distances on baseline CBCT scan with no restorations. Each difference shown is an average of nine measurements (GP-1, GP-2, GP-3 for 3 separate jaws), and displayed as average ± standard deviation.

3.5.2 Increased scan time

Table 14 shows the results when scanning time was 6.2 seconds and increased to 8.0 seconds. When compared to baseline CBCT measurements, the differences ranged from 0.01 ± 0.25 mm to 0.19 ± 0.60 mm at the lower scan time. Meanwhile, at the increased scan time, the differences ranged from 0.01 ± 0.25 mm to 0.46 ± 1.67 mm. The increase in scan time did not result in measurements that were statistically significant ($p>0.05$). The measurements were also not significantly different with increasing numbers of restorations, or when measured manually in three software packages (DTX, CS9300, and MicroView) ($p>0.05$ for all comparisons).

	Short Scan Time (6.2 sec)			Long Scan Time (8.0 sec)		
# of SSC	MicroView	DTX	Carestream	MicroView	DTX	Carestream
Left : 1	0.04 ± 0.44	0.16 ± 0.53	0.01 ± 0.54	0.29 ± 1.01	0.33 ± 0.95	0.27 ± 0.77
Left : 2	0.01 ± 0.40	0.06 ± 0.55	0.08 ± 0.60	0.07 ± 0.47	0.06 ± 0.43	0.01 ± 0.26
Left : 3	0.11 ± 0.32	0.19 ± 0.60	0.12 ± 0.59	0.04 ± 0.38	0.53 ± 1.65	0.09 ± 0.29
Left : 4	0.03 ± 0.37	0.06 ± 0.36	0.06 ± 0.57	0.12 ± 0.47	0.07 ± 0.39	0.04 ± 0.25
Right : 5	0.11 ± 0.34	0.01 ± 0.26	0.10 ± 0.30	0.03 ± 0.43	0.46 ± 1.67	0.02 ± 0.26
Right: 6	0.04 ± 0.45	0.05 ± 0.46	0.01 ± 0.35	0.09 ± 0.65	0.03 ± 0.28	0.01 ± 0.29
Right: 7	0.06 ± 0.41	0.05 ± 0.23	0.09 ± 0.33	0.02 ± 0.48	0.14 ± 0.42	0.29 ± 0.33
Right: 8	0.03 ± 0.34	0.01 ± 0.25	0.04 ± 0.37	0.05 ± 0.65	0.07 ± 0.36	0.16 ± 0.28

Table 14. Altered scan time groups. The difference in mm, between distances measured on CBCT images with increasing number of restorations, and distances on baseline CBCT scan with no restorations. Each difference shown is an average of nine measurements (GP-1, GP-2, GP-3 for 3 separate jaws), and displayed as average ± standard deviation.

3.6 Comparing software packages

When the manual measurements were repeated in the three software packages for amalgam restorations (DTX, CS9300, and MicroView), no statistically significant difference was found ($p>0.05$). Similarly, for SSC restorations, when the manual measurements were repeated in the three software packages (DTX, CS9300, and MicroView) no significant difference was found between the different software packages ($p>0.05$).

3.6.1 Manual and semi-automated measurements

There was a statistically significant difference between semi-automated MicroView and manual MicroView measurements ($p=0.022$), manual DTX measurements ($p<0.001$), and manual CS9300 ($p<0.001$). This was demonstrated only for the full arch FOV amalgam group only. The single site amalgam group, full arch SSC group, and single site SSC group did not show statistical significance between manual and semi-automated measurements. These results are listed as part of Tables 4 and 5 for amalgam restorations, and Tables 8 and 9 for SSC restorations.

Chapter 4: Discussion

In striving for optimally placed implants, pre-operative CBCT evaluation of the surgical site has become routine. There are currently no guidelines available that address the impact of artifact produced by metal restorations on that pre-operative evaluation. Routine CBCT imaging is performed, exposing the patient to radiation regardless of the expected image quality based on the number of metal restorations present, which can sometimes be on every tooth. In fact, it can be argued that patients with previous restorations, many of which are metal, are more likely to require implants than those without any restorations. Therefore, this is a common clinical scenario for which there are no current guidelines. Our study reports the novel finding that there was no significant difference in measurements made on CBCT images of an *in vitro* porcine model with a range of zero (0) to eight (8) metal restorations bilaterally. This was found to be true with amalgam and SSC restorations, different FOVs, under different scanning parameters, and measured on different software packages.

4.1 Caliper and baseline CBCT measurements

Comparing caliper measurements to baseline CBCT measurements, our study reports a mean difference of 0.60 ± 0.41 mm. This mean difference is similar to those reported by previous studies (21, 22, 25, 26, 34), regardless of the technique used to compare the measurements between a CBCT image and the subject measured by a caliper. A study of 10 dry mandibles reported a mean difference of 0.41 mm compared to digital caliper measurements (21), while another study performed on 13 dry mandibles showed a mean difference of 0.4 mm and 0.6 mm depending on the reference points of measurement they were using (22). Examples of studies with the soft tissue intact on their experimental model are also comparable, such as

one with 6 human cadaver heads reporting a mean difference of 0.3 mm (25), and another study also with 6 human cadaver heads showing a mean difference of up to 0.19 ± 0.84 mm (26). One study that had a similar design also used gutta percha points and porcine jaws to evaluate mean differences between measurements on the anatomic jaws and CBCT images (34). They evaluated 7 mandibles and found a mean difference of 0.45 ± 0.33 mm, and also reported a range of variation of 0 to 1.42 mm. These studies form the basis for the 2 mm zone of error applied by most programs and clinicians when planning a prospective implant case. The findings of our study are within that reported range, which is important to note since it indicates that our CBCT machine and commonly used settings produce results that are within expected limits.

4.2 Type of dental material, restoration surfaces, and FOV

Another important perspective on the findings of our study, is that only the full arch FOV with dental amalgam restorations showed a statistically significant result out of all of the variables explored. There are several important points to discuss pertaining to that result: the intrinsic properties of material (amalgam vs SSC), the type of tooth coverage (single surface vs full coverage), and the FOV. It has been well established in the literature that denser materials with higher atomic numbers result in more absorbed x-rays, and, therefore greater beam hardening (18). Greater beam hardening results in more noticeable metal artifact, which can be expected to have a greater effect on measurement accuracy. Dental amalgam is composed primarily of mercury, silver, tin, and zinc with high atomic numbers of 80, 47, 50, and 30 respectively. Meanwhile, metal crowns used in dentistry are divided by the American Dental Association (ADA) into three categories: *high-noble* with a required noble metal content of ≥60% and of which gold is ≥40%, *noble* with a noble metal composition of ≥25%, and

predominantly base metal with a noble metal content <25% (35). Fluctuations in the price of noble metals, in addition to tooth preparation and restoration design often determine which material is used. It is important to note, however, that these metals all have different atomic numbers and densities which may impact the artifact produced. For example, high noble crowns are composed mainly of gold (atomic number of 79) and other noble metals such as platinum or iridium with similarly high atomic numbers comparable to amalgam components (35). At the other end of the spectrum, base metals are composed of some combination of silver, copper, zinc, iron, and nickel which all have much lower atomic numbers and densities (35).

This study utilized stainless-steel crowns, which fall under the category of base metal crowns and are composed of primarily iron (atomic number 26, density of 7.87 g/cm^3) along with various compositions of carbon, chromium, nickel and other base metals (35). They are typically used in situations that require a preformed crown, such as in pediatrics or emergency situations, as opposed to a custom lab fabricated one. While the atomic number and density of these metals are similar to other base metals, it is not identical. This can be a potential limitation of this study in terms of application to everyday situations, because it can be rare to encounter a stainless-steel crown in an adult patient. The reasoning behind using stainless-steel crowns in this study was their availability in the dentistry setting, having various sizes easily accessible, and being able to mold them chairside to fit various sizes of porcine teeth which can vary considerably. An added factor as well was the significant difference in cost of a preformed crown as opposed to a customized lab fabricated one. An alternative type of crown that may be more applicable to adult clinical situations are zirconia crowns, which are primarily composed of zirconium with an atomic number of 40 that is comparable to most base metals and many amalgam components. Difficulty in accessing multiple sizes and shapes of these crowns at an

acceptable cost would be the main barrier, however, the possibility of lab milling makes them more accessible than many customizable metal crowns.

Vasconcelos et al. attempted to quantitatively compare metal artifact produced from different materials by calculating the standard deviation of gray values in voxels surrounding the artifact producing object (36). They found that dental amalgam (with the highest atomic number) produced the greatest artifact expression, followed by copper-aluminum alloy, and finally titanium (with the lowest atomic number). Another study used the same technique of calculating the standard deviation of gray values around dental materials, comparing dental amalgam, aluminum-copper alloy, and gutta percha (37). They reported a statistically significant difference for both metal alloys but not the gutta percha when compared to their controls of areas with dental material. The authors explained these findings also by referring to the atomic number and density of the material; gutta percha is composed of primarily isoprene rubber which has a very low atomic number, in addition to zinc oxide.

There are currently no studies in the literature addressing different types of tooth coverage and the impact on metal artifact, let alone measurement accuracy. It stands to reason that if the material type is the same, larger or thicker restorations would produce more metal artifact. One way to address the amount of material question would be through the number of tooth surfaces covered; for example, single surface restorations such as occlusal amalgams used in this study, as opposed to three or four surface restorations. Stainless steel crowns cover all surfaces, however, introduce another variable in material type, making it difficult to directly compare the effect of larger tooth surface coverage only. Another way to address the same question is through the amount of material by weight, which may in fact be less for full coverage restorations since they are often only 0.8-1.0 mm in width. Our study seems to indicate that even

though the SSC restorations are full coverage, surfaces covered may not be the most important aspect, either due to the material itself or the type of tooth coverage. Since it appears that amalgam may produce more artifact expression, perhaps larger multi-surface amalgam restorations as opposed to the single surface restorations used in this study can be a future area of research.

Our study reports measurements on CBCT images with restorations, that were significantly different when compared to caliper measurements for the full arch (10x5 cm) amalgam group only, not the single site (5x5 cm) amalgam group. A likely explanation for the discrepancy in findings between the two FOV sizes is the greater amount of scatter produced by larger FOVs. Greater amounts of scatter produce a lower quality image, which would explain why there might be a significant difference in measurements made on those images. This has been documented in the literature by Pauwels et al, who report that smaller FOVs produce significantly less scatter than larger FOVs (38). However, other studies addressing metal artifact and FOV size have reported inconsistent findings. A study by Codari et al. quantitatively compared metal artifact produced by high-density materials and FOV size by measuring volume differences between CBCT images of phantoms. They reported that images with amalgam pins placed in the phantoms produced significantly different volumes compared to the true volumes by up to 67%. The amalgam group showed the greatest volume difference, followed by the other groups which were similar, titanium and copper-aluminum alloy. The authors explain the difference in material type by referring to the high atomic number of amalgam components compared to the other materials, similar to our study. Regarding FOV size, however, they reported no significant difference in volume with a "medium" FOV (10 x 5 cm) compared to a "small" FOV (5 x 5 cm). Making the connection between increased scatter due to larger FOVs,

reduced image quality, and therefore a greater discrepancy in measurements seems logical, however, requires further evidence than currently available.

4.3 Metal artifact and measurement accuracy

Even though our study reports that there may be some impact in the full arch FOV amalgam group when compared to the caliper measurements, no change in measurement accuracy was observed when compared to the baseline scans. The comparison with baseline images removes the impact of caliper to CBCT image differences, and simply compares the CBCT images with progressively increasing metal restorations. The main take home message from this type of analysis is that there is no added impact of the metal artifact causing a change in measurement accuracy beyond what can be expected due to chance. It is important to note from a clinical perspective that the maximum difference observed was 0.54 ± 0.64 mm for amalgam restorations and 0.62 ± 0.64 mm for the SSC restorations; however, according to the findings of our study, that difference can happen in measurements between multiple CBCT images with or without metal restorations.

To date, there are two published *in vitro* studies addressing metal artifact and specifically measurement accuracy on CBCT images (39, 40). Kim et al. sought to address this problem from the perspective of accuracy of implant placement through a surgical guide designed via the CBCT images. The accuracy of implant placement on mandibular cast models with no restorations was compared to those with six (6) and eight (8) metal crowns. They reported a variation from the digitally planned implants at entry of 0.55 ± 0.29 mm for the group with no restorations, and a variation of 0.87 ± 0.31 mm for the group with eight (8) restorations. That difference between the groups was reported to be statistically significant for measurements made

in regards to implant location at the implant shoulder, apex, depth, and angulation. While the mean differences reported are similar to those obtained in this study, the finding of statistical significance is not. One possible explanation may be that the process of superimposing the CBCT image with metal artifact to a digital model may be a more distortion sensitive process than the linear measurements made in this study. The other factor to consider is that the difference between both group means is 0.32 mm which is similar to the variations observed in our study, and while statistically significant, may not be clinically significant. Another important aspect in the study by Kim et al. is that the authors did not report what type of metal crowns were placed, which as discussed above is relevant in a study addressing metal artifact.

4.4 Improved image quality approaches using altered CBCT scan parameters

Our study reports no significant difference with increased peak kilovoltage or scan time. Both of those variables would be expected to produce metal artifact reduction based on increasing the beam quality and the number of x-rays, respectively (29). There are several ways to interpret our findings. It may be that there is in fact no metal artifact reduction because the increase in peak kilovoltage or scan time was not sufficient to detect a difference. Or, more likely, there was an improvement in the metal artifact, however, that did not translate to an improvement in measurement accuracy. Vasconcelos et al. looked at the issue of metal artifact and the impact of MAR approaches on measurement accuracy (36). The authors evaluated distances measured on a CBCT image of dry mandibles from the apex of artifact producing titanium and zirconia implants to a known axial reference line. They compared these distances to controls measured from an area on the CBCT image that they termed “over the water”, or away from the implants. No mean differences were reported, but they reported standard

deviations of the grey scale values that were significantly higher to the controls. Higher kVp and the use of a built-in MAR tool on the CBCT were shown to decrease these standard deviation values. The authors used two different CBCT machines, one of which had higher peak kilovoltage and beam intensity, and produced improved results in terms of reducing the metal artifact. The results of this study are difficult to directly correlate to the findings of our study because they increase both beam intensity and peak kilovoltage; however, they show an interest in evaluating a similar problem from the perspective of the impact of metal artifact affecting measurement accuracy CBCT scans.

4.5 Manual and semi-automated measurements

The rationale for calculating the semi-automated points using MicroView and comparing them to manual measurements in MicroView, DTX, and CS9300 was to address a possible source of error in the selection of consistent points of measurement by eye. It was found that there was a statistically significant difference between semi-automated and manual MicroView measurements for the full arch FOV amalgam restorations group ($p=0.022$). Semi-automated MicroView measurements were also found to be statistically significant to those made manually on DTX ($P<0.001$) and CS9300 ($p<0.001$). The fact that both manual and semi-automated MicroView measurements were more accurate than manual measurements on DTX and CS9300, seem to indicate that there may be an added benefit to using a software with increased functionality such as MicroView, especially in the presence of metal artifact such as amalgam. Features of that program that were especially helpful, were the ease of navigation around the metal artifacts in the different projections, and greater magnification capability allowing visualization of the region of interest more clearly. The use of semi-automated measurements as

opposed to manual measurements also showed improved accuracy compared to manual DTX and CS9300 measurements. This is possibly due to an aspect of human based error in selecting the points, which may have been minimized by the semi-automated measurements. However, even though these measurements on MicroView seemed to perform better, there was no trend with increasing number of metal restorations. Greater software functionality, magnification, and the use of semi-automated landmark identification are all concepts that can be explored further in future studies.

4.6 Sources of error and future directions

In a study addressing measurement accuracy, it is expected that there will be an aspect of human error in reliably selecting measurement points. To address this issue and realistically reproduce clinical scenarios, several software packages were used for measurement. Based on the results of our study, there is some evidence that greater functionality and magnification, in addition to semi-automated selection may be beneficial in improving measurement accuracy on CBCT images, especially in the presence of dental amalgam in a full arch FOV. While software functionality and magnification can be easily improved, semi-automated landmark identification requires technology that is not currently available chairside. However, this may be an important area of research worth pursuing in the future.

Another possible source of error in this study is the use of gutta percha points, which themselves are radiopaque and will produce some level of scatter. The rationale for using the gutta percha points was to provide a consistent point of measurement that was easy to identify and allowed for reliability in selecting the same point on the CBCT image. However, the tradeoff in using a radiopaque marker is that identifying those points on the CBCT images may

be less likely to be impacted by adjacent artifact from the restorations since markers are themselves highly attenuating. One would expect greater metal artifact produced overall with more radiopaque material (gutta percha) present in addition to the restorations. However, in terms of evaluating measurement accuracy, this can be expected to underestimate the impact of the metal artifact because these points are much easier to identify since they are radiopaque relative to the bone. In clinical situations, the alveolar ridge and other relevant anatomy is typically more radiolucent and subtler to identify, and therefore may be more likely to be impacted by adjacent metal artifact. A possible solution for this in future studies can be to use small notches created by a highspeed handpiece on the ridge itself as a reliable point of measurement. These notches would not interfere with the amount of artifact produced, but also be easily identifiable on the CBCT images. Addressing scatter within the bone, directly adjacent to the measurement points, is an idea that can be further explored in future research as well. Titanium implants within the alveolar process is an increasingly common occurrence, and measurement accuracy directly adjacent to those implants will be directly affected by some of the same issues addressed in this study.

A third challenge that may have impacted the results is in the measurement of the anatomic distances with the digital caliper. An effort was made to select the gutta percha points carefully for measurement with the caliper, however, it was often difficult to fit the caliper with precision on the small gutta percha point due to the size of the jaw. The study by Halperin-Sterfield et al. had a similar study design with porcine jaws and gutta percha points as well, and they circumvented this problem by sectioning the porcine mandibles using a band saw at the level of the gutta percha points after they were scanned. This facilitated accurate and reliable

measurement with the digital caliper (34). While the results of our study are similar, this extra step may be beneficial in future studies.

4.7 Clinical perspective

From a clinical perspective, the findings of this study first of all confirm that there is often a difference between caliper (or clinical) measurements and measurements on a CBCT image of up to 1.7 mm, which is similar to previous studies. There was no attributable increase in these measurements with increasing numbers of metal restorations, which supports current clinical guidelines. There is no evidence that patients with multiple restorations would not benefit from a pre-operative CBCT image analysis of their prospective implant site compared to a patient with no metal restorations. Software packages and current clinical practice typically assumes a difference between any CBCT image and anatomy that may be up to 2.0 mm, and this was found to be no different in this study for situations with or without metal restorations. There may be some benefit to using a specialized imaging software enabling greater optimization of the images and magnification when there are many highly dense dental materials, such as amalgam, in a full arch FOV. Future studies are needed to correlate these findings with the next step in the clinical workflow of implant dentistry, which is surgical guide fabrication.

Chapter 5: Conclusion

The goal of this study was to assess the impact of progressively increasing metal restorations on measurement accuracy of commonly evaluated points in CBCT. Several variables such as the FOV, type of restoration, and software used to evaluate the measurements were introduced. This study reports no significant difference in measurements made on an *in vitro* experimental porcine model with up to eight (8) metal restorations bilaterally. There was a variation of less than 2 mm from the true anatomy as measured by a caliper, however, that variation was not shown to increase with the number of metal restorations present. When compared to scans taken with no restorations placed, scans with metal restorations showed a maximum variation of 0.54 ± 0.64 mm for amalgam restorations and 0.62 ± 0.64 mm for the SSC restorations. This was found to be true for both single surface amalgam restorations and full coverage SSCs. While these differences are not statistically significant from the measurements on the baseline scans, the maximum amount of variation found is important to note from a clinical perspective. When these measurements were repeated on three different software packages, there was a significant difference between semi-automated and manual measurements on MicroView compared to manual measurements on the other software packages. This significant result was found only in the full arch amalgam group. Finally, changes in the FOV or CBCT scan settings to increase kilovoltage and scan time did not result in a significant difference. This study supports current clinical guidelines which do not limit the use of CBCT imaging in the presence of metal restorations. It also supports previous research which has shown a variation of measurements made on CBCT images compared to anatomy of less than 2 mm, which is relevant from a clinical perspective.

Bibliography

1. De Bruyn H, Vandeweghe S, Ruyffelaert C, Cosyn J, Sennerby L. Radiographic evaluation of modern oral implants with emphasis on crestal bone level and relevance to peri-implant health. Periodontol 2000. 2013;62(1):256-70.
2. Figuero E, Graziani F, Sanz I, Herrera D, Sanz M. Management of peri-implant mucositis and peri-implantitis. Periodontol 2000. 2014;66(1):255-73.
3. Schwarz F, Sahm N, Iglhaut G, Becker J. Impact of the method of surface debridement and decontamination on the clinical outcome following combined surgical therapy of peri-implantitis: a randomized controlled clinical study. J Clin Periodontol. 2011;38(3):276-84.
4. Salvi GE, Cosgarea R, Sculean A. Prevalence and Mechanisms of Peri-implant Diseases. J Dent Res. 2017;96(1):31-7.
5. Derks J, Tomasi C. Peri-implant health and disease. A systematic review of current epidemiology. J Clin Periodontol. 2015;42 Suppl 16:S158-71.
6. Sanz M, Noguerol B, Sanz-Sanchez I, Hammerle CHF, Schliephake H, Renouard F, et al. European Association for Osseointegration Delphi study on the trends in Implant Dentistry in Europe for the year 2030. Clin Oral Implants Res. 2019;30(5):476-86.
7. Tyndall DA, Price JB, Tetradis S, Ganz SD, Hildebolt C, Scarfe WC, et al. Position statement of the American Academy of Oral and Maxillofacial Radiology on selection criteria for the use of radiology in dental implantology with emphasis on cone beam computed tomography. Oral Surg Oral Med Oral Pathol Oral Radiol. 2012;113(6):817-26.
8. Kalpidis CD, Setayesh RM. Hemorrhaging associated with endosseous implant placement in the anterior mandible: a review of the literature. J Periodontol. 2004;75(5):631-45.
9. Zijderveld SA, van den Bergh JP, Schulten EA, ten Bruggenkate CM. Anatomical and surgical findings and complications in 100 consecutive maxillary sinus floor elevation procedures. J Oral Maxillofac Surg. 2008;66(7):1426-38.
10. Renton T, Dawood A, Shah A, Searson L, Yilmaz Z. Post-implant neuropathy of the trigeminal nerve. A case series. Br Dent J. 2012;212(11):E17.
11. The 2007 Recommendations of the International Commission on Radiological Protection. ICRP publication 103. Ann ICRP. 2007;37(2-4):1-332.
12. Pauwels R, Araki K, Siewerdsen JH, Thongvigitmanee SS. Technical aspects of dental CBCT: state of the art. Dentomaxillofac Radiol. 2015;44(1):20140224.
13. Kiljunen T, Kaasalainen T, Suomalainen A, Kortesniemi M. Dental cone beam CT: A review. Phys Med. 2015;31(8):844-60.
14. Ludlow JB, Timothy R, Walker C, Hunter R, Benavides E, Samuelson DB, et al. Effective dose of dental CBCT-a meta analysis of published data and additional data for nine CBCT units. Dentomaxillofac Radiol. 2015;44(1):20140197.
15. Abouei E, Lee S, Ford NL. Quantitative performance characterization of image quality and radiation dose for a CS 9300 dental cone beam computed tomography machine. J Med Imaging (Bellingham). 2015;2(4):044002.
16. Pauwels R, Stamatakis H, Manousaridis G, Walker A, Michielsen K, Bosmans H, et al. Development and applicability of a quality control phantom for dental cone-beam CT. J Appl Clin Med Phys. 2011;12(4):3478.
17. Pauwels R, Jacobs R, Singer SR, Mupparapu M. CBCT-based bone quality assessment: are Hounsfield units applicable? Dentomaxillofac Radiol. 2015;44(1):20140238.

18. Schulze R, Heil U, Gross D, Bruellmann DD, Dranischnikow E, Schwanecke U, et al. Artefacts in CBCT: a review. Dentomaxillofac Radiol. 2011;40(5):265-73.
19. Makins SR. Artifacts interfering with interpretation of cone beam computed tomography images. Dent Clin North Am. 2014;58(3):485-95.
20. Jekel JF. Epidemiology, biostatistics, and preventive medicine. Philadelphia, PA: Saunders Elsevier; 2007. p. 105-106.
21. Fernandes TM, Adamczyk J, Poleti ML, Henriques JF, Friedland B, Garib DG. Comparison between 3D volumetric rendering and multiplanar slices on the reliability of linear measurements on CBCT images: an in vitro study. J Appl Oral Sci. 2015;23(1):56-63.
22. Leung CC, Palomo L, Griffith R, Hans MG. Accuracy and reliability of cone-beam computed tomography for measuring alveolar bone height and detecting bony dehiscences and fenestrations. Am J Orthod Dentofacial Orthop. 2010;137(4 Suppl):S109-19.
23. Menezes CC, Janson G, da Silveira Massaro C, Cambiaghi L, Garib DG. Precision, reproducibility, and accuracy of bone crest level measurements of CBCT cross sections using different resolutions. Angle Orthod. 2016;86(4):535-42.
24. Kwong JC, Palomo JM, Landers MA, Figueroa A, Hans MG. Image quality produced by different cone-beam computed tomography settings. Am J Orthod Dentofacial Orthop. 2008;133(2):317-27.
25. Ganguly R, Ruprecht A, Vincent S, Hellstein J, Timmons S, Qian F. Accuracy of linear measurement in the Galileos cone beam computed tomography under simulated clinical conditions. Dentomaxillofac Radiol. 2011;40(5):299-305.
26. Garcia-Sanz V, Bellot-Arcis C, Hernandez V, Serrano-Sanchez P, Guarinos J, Paredes-Gallardo V. Accuracy and Reliability of Cone-Beam Computed Tomography for Linear and Volumetric Mandibular Condyle Measurements. A Human Cadaver Study. Sci Rep. 2017;7(1):11993.
27. Behnia H, Motamedian SR, Kiani MT, Morad G, Khojasteh A. Accuracy and reliability of cone beam computed tomographic measurements of the bone labial and palatal to the maxillary anterior teeth. Int J Oral Maxillofac Implants. 2015;30(6):1249-55.
28. MacDonald D. Oral and Maxillofacial Radiology: A Diagnostic Approach. 2nd Edition ed: Wiley-Blackwell; 2019. p. 84.
29. Bechara BB, Moore WS, McMahan CA, Noujeim M. Metal artefact reduction with cone beam CT: an in vitro study. Dentomaxillofac Radiol. 2012;41(3):248-53.
30. Tohnak S, Mehnert AJ, Mahoney M, Crozier S. Dental CT metal artefact reduction based on sequential substitution. Dentomaxillofac Radiol. 2011;40(3):184-90.
31. de-Azevedo-Vaz SL, Peyneau PD, Ramirez-Sotelo LR, Vasconcelos Kde F, Campos PS, Haiter-Neto F. Efficacy of a cone beam computed tomography metal artifact reduction algorithm for the detection of peri-implant fenestrations and dehiscences. Oral Surg Oral Med Oral Pathol Oral Radiol. 2016;121(5):550-6.
32. Vasconcelos KF, Nicolielo LF, Nascimento MC, Haiter-Neto F, Boscolo FN, Van Dessel J, et al. Artefact expression associated with several cone-beam computed tomographic machines when imaging root filled teeth. Int Endod J. 2015;48(10):994-1000.
33. Stembirek J, Kyllar M, Putnova I, Stehlik L, Buchtova M. The pig as an experimental model for clinical craniofacial research. Lab Anim. 2012;46(4):269-79.

34. Halperin-Sternfeld M, Machtei EE, Horwitz J. Diagnostic accuracy of cone beam computed tomography for dimensional linear measurements in the mandible. Int J Oral Maxillofac Implants. 2014;29(3):593-9.
35. Sakaguchi RL, Powers JM. Craig's Restorative Dental Materials. 12th ed. Philadelphia, PA: Elsevier Mosby; 2012 p. 368-369.
36. Vasconcelos KF, Codari M, Queiroz PM, Nicolielo LFP, Freitas DQ, Sforza C, et al. The performance of metal artifact reduction algorithms in cone beam computed tomography images considering the effects of materials, metal positions, and fields of view. Oral Surg Oral Med Oral Pathol Oral Radiol. 2019;127(1):71-6.
37. Queiroz PM, Oliveira ML, Groppo FC, Haiter-Neto F, Freitas DQ. Evaluation of metal artefact reduction in cone-beam computed tomography images of different dental materials. Clin Oral Investig. 2018;22(1):419-23.
38. Pauwels R, Jacobs R, Bogaerts R, Bosmans H, Panmekiate S. Reduction of scatter-induced image noise in cone beam computed tomography: effect of field of view size and position. Oral Surg Oral Med Oral Pathol Oral Radiol. 2016;121(2):188-95.
39. Kim JE, Park YB, Shim JS, Moon HS. The Impact of Metal Artifacts Within Cone Beam Computed Tomography Data on the Accuracy of Computer-Based Implant Surgery: An In Vitro Study. Int J Oral Maxillofac Implants. 2019;34(3):585-94.
40. Vasconcelos TV, Leandro Nascimento EH, Bechara BB, Freitas DQ, Noujeim M. Influence of Cone Beam Computed Tomography Settings on Implant Artifact Production: Zirconia and Titanium. Int J Oral Maxillofac Implants. 2019;34(5):1114-20.